Plant Communications
Research article

CellPress
Partner Journal

The trxG protein ULT1 regulates *Arabidopsis* organ size by interacting with TCP14/15 to antagonize the LIM peptidase DA1 for H3K4me3 on target genes

Fan Xu[1,5], Huixue Dong[2,5], Weijun Guo[1], Liang Le[1], Yexing Jing[2], Jennifer C. Fletcher[3,4], Jiaqiang Sun[2,*] and Li Pu[1,*]

[1]Biotechnology Research Institute, Chinese Academy of Agricultural Sciences, Beijing 100081, China

[2]State Key Laboratory of Crop Gene Resources and Breeding, Institute of Crop Sciences, Chinese Academy of Agricultural Sciences, Beijing 100081, China

[3]Department of Plant and Microbial Biology, University of California, Berkeley, Berkeley, CA 94720, USA

[4]Plant Gene Expression Center, United States Department of Agriculture – Agricultural Research Service, Albany, CA 94710, USA

[5]These authors contributed equally to this article.

***Correspondence: Jiaqiang Sun (sunjiaqiang@caas.cn), Li Pu (puli@caas.cn)**

https://doi.org/10.1016/j.xplc.2024.100819

ABSTRACT

Plant organ size is an important agronomic trait that makes a significant contribution to plant yield. Despite its central importance, the genetic and molecular mechanisms underlying organ size control remain to be fully clarified. Here, we report that the trithorax group protein ULTRAPETALA1 (ULT1) interacts with the TEOSINTE BRANCHED1/CYCLOIDEA/PCF14/15 (TCP14/15) transcription factors by antagonizing the LIN-11, ISL-1, and MEC-3 (LIM) peptidase DA1, thereby regulating organ size in *Arabidopsis*. Loss of *ULT1* function significantly increases rosette leaf, petal, silique, and seed size, whereas overexpression of *ULT1* results in reduced organ size. ULT1 associates with TCP14 and TCP15 to co-regulate cell size by affecting cellular endoreduplication. Transcriptome analysis revealed that ULT1 and TCP14/15 regulate common target genes involved in endoreduplication and leaf development. ULT1 can be recruited by TCP14/15 to promote lysine 4 of histone H3 trimethylation at target genes, activating their expression to determine final cell size. Furthermore, we found that ULT1 influences the interaction of DA1 and TCP14/15 and antagonizes the effect of DA1 on TCP14/15 degradation. Collectively, our findings reveal a novel epigenetic mechanism underlying the regulation of organ size in *Arabidopsis*.

Key words: ULT1, TCP, DA1, organ size, endoreduplication

Xu F., Dong H., Guo W., Le L., Jing Y., Fletcher J.C., Sun J., and Pu L. (2024). The trxG protein ULT1 regulates *Arabidopsis* organ size by interacting with TCP14/15 to antagonize the LIM peptidase DA1 for H3K4me3 on target genes. Plant Comm. **5**, 100819.

INTRODUCTION

The size of plant organs is important in agriculture because larger organs can result in increased crop biomass and overall yield. Organ size is coordinately determined by initial cell division and subsequent cell expansion until the final size is reached (Gonzalez et al., 2012). Unlike animals, which form the rudiments of organs in embryos, plant seeds germinate and then develop leaves, stems, and flowers by cell division and cell differentiation within the stem cell niche of the apical meristems (Chen and Laux, 2012). Thus, the activity and maintenance of meristem cells influence final plant organ size (Schnablova et al., 2017). For example, in *Arabidopsis*, *PEAPOD 1* and *PEAPOD 2* restrain leaf size by promoting the early arrest of dispersed meristematic cells (White, 2006; Wang et al., 2016).

Cell division makes a significant contribution to organ size by affecting cell number. A number of genes play positive roles in regulating cell division, such as *AINTEGUMENTA*, *ANGUSTIFOLIA 3*, *ERECTA*, *GROWTH-REGULATING FACTOR 5* (*GRF5*), *JAGGED*, *STRUWWELPETER*, and *SWELLMAP 1* (Krizek, 1999; Mizukami

Published by the Plant Communications Shanghai Editorial Office in association with Cell Press, an imprint of Elsevier Inc., on behalf of CSPB and CEMPS, CAS.

and Fischer, 2000; Autran et al., 2002; Dinneny et al., 2004; Shpak et al., 2004; Clay and Nelson, 2005; Horiguchi et al., 2005; Kawade et al., 2013). They prolong the duration of cell division to produce larger organs with more cells. By contrast, other genes restrict organ size by limiting the period of cell proliferation (Li et al., 2008; Xia et al., 2013). In *Arabidopsis*, *DA1* encodes a ubiquitin receptor and is the most representative gene in the ubiquitination pathway responsible for negatively mediating organ size (Li et al., 2008). Homologs of DA1 also play vital roles in the regulation of grain size in maize and rice (Xie et al., 2018; Gao et al., 2021). Two RING-type E3 ubiquitin ligases, DA2 and BIG BROTHER (BB), physically interact with DA1, and mutations in these two genes can synergistically enhance seed- and organ-size phenotypes of *da1-1* (Disch et al., 2006; Xia et al., 2013; Vanhaeren et al., 2017). Both DA2 and BB can monoubiquitinate DA1 at multiple sites, activating its peptidase activity (Xia et al., 2013; Dong et al., 2017). Cell expansion also makes a large contribution to final organ size. Cytoskeletal components, such as F-actin and microtubule-associated proteins, are required for growth by cell expansion and shape the direction of expansion (Wu and Bezanilla, 2018). Cell wall modification and structure can also directly affect cell expansion (Sasidharan and Pierik, 2010). For example, expansins are a class of plant-conserved proteins that loosen cell walls to mediate cell expansion under acidic growth conditions (Cosgrove, 2000; Ma et al., 2013). Some transcription factors (TFs) also regulate organ size through cell expansion. GRF1/2 play an important role in regulating leaf cell expansion (Kim et al., 2003). BIG PETALp is a key negative regulator of petal cell expansion whose functions are relevant to the floral industry (Szecsi et al., 2006). In addition, cell endoreduplication, during which DNA replication occurs in the absence of cytokinesis, can increase plant cell size (Sugimoto-Shirasu and Roberts, 2003). The deregulation of some cyclins and cyclin-dependent kinases, such as CYCA2;3, CYCD3;1 and CDKB1;1 (Dewitte et al., 2003; Imai et al., 2006; Boudolf et al., 2009), initiates endoreduplication (Wuarin et al., 2002). CELL CYCLE SWITCH 52 (CCS52) promotes the degradation of CYCA and CDKB1;1 by the ANAPHASE-PROMOTING COMPLEX/CYCLOSOME (APC/C) complex (Willems et al., 2020). The TF E2F can bind to and activate the expression of *CCS52* (Lammens et al., 2008), and RETINOBLASTOMA-RELATED 1 (RBR1) is an ortholog of RETINOBLASTOMA (Rb) in mammals that regulates the cell cycle by interacting with the E2Fa/DRTF 1-POLYPEPTIDE (DP) TF to prevent expression of *CCS52* (Magyar et al., 2012). Two families of CYCLIN-DEPENDENT KINASES (CDK) inhibitors, INHIBITOR/INTERACTOR OF CYCLIN-DEPENDENT KINASES/KIP-RELATED PROTEIN (ICK/KRP) and SIAMESE/SIAMESE-RELATED (SIM/SMR), are also positive regulators of cell endoreduplication (Wang et al., 1997; Churchman et al., 2006). DA1 and DA1-related proteins have also been shown to redundantly regulate leaf cell endoreduplication and control organ size in *Arabidopsis* (Peng et al., 2015).

In multicellular organisms, DNA-binding TFs as well as epigenetic regulators cooperatively play crucial roles in various developmental programs and establishment of cell fates. Trithorax group (trxG) factors function in epigenetic protein complexes that can regulate transcriptional activation through trimethylation of lysine 4 of histone H3 (H3K4me3). In plants, the trxG complex participates in various developmental processes from embryogenesis to floral development, regulating the expression of several TFs involved in stem cell maintenance, cell fate identity, and cell proliferation and differentiation (de la Paz Sanchez et al., 2015; Fletcher, 2017). ULTRAPETALA 1 (ULT1), a plant transcriptional regulatory protein identified as a trxG factor, has multiple developmental roles, including regulation of shoot and floral meristem activity (Carles et al., 2005). ULT1 is a SAND (Sp100, AIRE-1, NucP41/75, DEAF-1)-domain-containing protein that can bind via this domain to a GAGAG motif present in Polycomb response elements (PREs), which can be recognized by both Polycomb group (PcG) factors and trxG factors (Roy et al., 2019). *ULT1* is expressed in shoot and floral meristems as well as in developing organs; its loss of function increases shoot and floral stem cell accumulation and delays floral meristem determinacy, producing supernumerary flowers and floral organs (Carles et al., 2004, 2005). Although ULT1 lacks enzymatic activity (Saleh et al., 2007), as a coactivator of ARABIDOPSIS TRITHORAX 1 (ATX1), ULT1 can physically interact with ATX1 to control the transcriptional activation of target genes such as *AGAMOUS* by stimulating H3K4me3 deposition and antagonizing the activity of CURLY LEAF, a histone methyltransferase component of the PcG repressor complex (Carles and Fletcher, 2009). ULT1 also regulates other MADS-box and class 1 *KNOX* genes involved in the maintenance of aerial meristems (Monfared et al., 2013). In our previous study, we showed that ULT1 interacts with ATX1 to form a complex with a plant-specific PcG protein, EMBRYONIC FLOWER 1, to maintain trimethylation of lysine 27 of histone H3 (H3K27me3) marks and a repressive chromatin state during germination (Xu et al., 2018a). A recent study has shown that ULT1 maintains quiescent center quiescence and modulates auxin signaling required for columella stem cell maintenance in roots (Ornelas-Ayala et al., 2020). Although ULT1 regulates diverse developmental and physiological processes, the underlying molecular mechanisms have not been fully clarified. Specific TFs, long non-coding RNAs, and other proteins have been shown to recruit PcG and trxG members to specific target loci for gene silencing or activation (Heo and Sung, 2011; Wu et al., 2012; Forderer et al., 2016; Kim and Sung, 2017; Tian et al., 2019; Yuan et al., 2021). However, only a few factors that specifically recruit ULT1 to the chromatin of target loci have been reported to date. ULT1 can interact with the GOLDEN2, ARR-B, PSR1 (GARP) domain TF KANADI 1 to establish apical–basal polarity by promoting basal cell fate in the gynoecium (Pires et al., 2014) and with the V-MYB AVIAN MYELOBLASTOSIS VIRAL ONCOGENE HOMOLOG (MYB) domain-containing TF ULTRAPETALA-INTERACTING FACTOR 1 to co-repress expression of *WUSCHEL* in the floral meristem (Moreau et al., 2016). However, given the diversity of its biological functions, additional recruiters of ULT1 to specific target genes are likely to exist.

To further investigate the genetic and molecular mechanisms of organ size determination, we determined the function of ULT1 in organ size control in *Arabidopsis*. Phenotypic analysis of *ULT1* null mutants and overexpression (OE) lines revealed that *ULT1* is both necessary and sufficient to restrict vegetative and reproductive organ size. Two members of the plant growth-regulating TEOSINTE BRANCHED1/CYCLOIDEA/PCF (TCP) TF family, TCP14 and TCP15, have been shown to physically interact with ULT1. Transcriptome analysis revealed that ULT1 and TCP14/15 share a large set of overlapping target genes that are specifically involved in endoreduplication, cell division, and leaf

development, and ULT1 acts genetically with TCP14/15 to modulate cell size by regulating the endoreduplication process. Chromatin immunoprecipitation (ChIP) analysis revealed a previously undescribed function for TCP14/15 in recruiting ULT1 to specific target genes to promote H3K4me3 deposition and increase their transcription levels. Interestingly, ULT1 might compete with the LIN-11, ISL-1, and MEC-3 (LIM) peptidase DA1 to interact with TCP14/TCP15 and protect TCP14/15 from degradation by DA1 in *Arabidopsis*. Together, our findings reveal the ULT1–TCP14/15 module as a novel epigenetic regulatory mechanism for control of organ size in plants.

RESULTS

ULT1 negatively regulates organ size in *Arabidopsis*

Our studies and other previous studies have shown that *ult1* plants form abnormally large petals and supernumerary flowers (Carles et al., 2005; Pu et al., 2013; Xu et al., 2018a). Here, we further investigated the function of ULT1 in regulating organ size using the transfer DNA insertion null mutant *ult1-3* (*ult1*) and *35S::ULT1-FLAG* OE transgenic plants (*ULT1-OE*). ULT1 mRNA and protein levels in transgenic lines were examined by quantitative reverse-transcription PCR (RT–qPCR) and western blot analysis. *ULT1* mRNA and protein levels were significantly higher in transgenic plants than in wild-type (WT) plants, confirming *ULT1* OE in the *Arabidopsis* transgenic lines (Supplemental Figure 1A and 1B). Compared with WT plants, *ULT1* mutation caused larger plant phenotypes, whereas transgenic plants overexpressing *ULT1* displayed smaller phenotypes under normal growth conditions (Figure 1A–1F and Supplemental Figure 1C–1F). The *ult1* plants produced larger cotyledons, rosette leaves, flowers, siliques, and seeds compared with those of WT plants, whereas *ULT1-OE* plants displayed smaller organ size (Figure 1A–1F and Supplemental Figure 1C–1F). Mature *ult1* plants were significantly taller than WT plants, with fewer branches, whereas the OE lines were shorter with more branches (Figure 1F). Consistent with these findings, the rosette diameter was 14.8% larger in *ult1 plants than in* WT plants but 41.3% smaller in *ULT1-OE* plants (Figure 1G). The number of rosette leaves was 41.5% greater in *ult1 plants* than in WT plants but 27.2% lower in *ULT1-OE* plants (Figure 1H). Both the *ult1* mutant and *ULT1-OE* plants showed statistically significant differences from the WT in cotyledon size, petal area, silique length, plant height, seed length, seed width, seed area, and thousand-seed weight (Figure 1I–1N and Supplemental Figure 1G–1I), demonstrating that *ULT1* is both necessary and sufficient to negatively regulate vegetative and reproductive organ size in *Arabidopsis*.

ULT1 physically interacts with the TCP14 and TCP15 TFs

TFs have been reported to recruit epigenetic regulators to target genes in plants (Heo and Sung, 2011; Wu et al., 2012; Hecker et al., 2015; Li et al., 2016; Yuan et al., 2021). To identify possible TFs interacting with ULT1, we used yeast two-hybrid (Y2H) assays to search for ULT1 partners from an *Arabidopsis* TF library containing a sequence-verified collection of 1581 full-length *Arabidopsis* TF clones (Ou et al., 2011). Using the ULT1 full-length protein as the bait, we identified two TFs, TCP14 and TCP15, as ULT1 interactors in yeast cells (Figure 2A). In *Arabidopsis*, the TCP TF family consists of 24 proteins with a highly conserved TCP domain, which are divided into 2 subclasses: class I with 13 members and class II with 11 members (Supplemental Figure 2). The TCP14 and TCP15 proteins belong to the TCP class I subclass of plant-specific TFs, which has been reported to regulate plant growth and development by influencing cell proliferation and cell differentiation (Kieffer et al., 2011; Peng et al., 2015; Dong et al., 2017). The TCP14 and TCP15 proteins, which share close sequence homology and show functional overlap (Kieffer et al., 2011), were also found to interact with one another in yeast cells (Figure 2A). We verified the interaction between ULT1 and TCP14/15 *in planta* using several methods. First, firefly luciferase (LUC) complementation imaging (LCI) assays were performed in *Nicotiana benthamiana* (Figure 2B). TCP14 and TCP15 were independently fused to the C-terminal part of LUC to produce the cLUC-TCP14 and cLUC-TCP15 constructs, and ULT1 was fused to the N-terminal part of LUC to generate the nLUC-ULT1 construct. When cLUC-TCP14 and nLUC-ULT1 were co-expressed in *N. benthamiana* leaves, strong LUC activity was detected (Figure 2B), verifying the interaction between ULT1 and TCP14. LUC activity was also found in *N. benthamiana* leaves co-infiltrated with cLUC-TCP15 and nLUC-ULT1 (Figure 2B). Second, we performed pull-down assays that confirmed the interaction between ULT1 and TCP14/TCP15 *in vivo* (Figure 2C and 2D). Third, co-immunoprecipitation (coIP) was used to validate the interaction between ULT1 and TCP *in vivo* by extracting proteins from *35S::ULT1-FLAG* plants and *35S::ULT1-FLAG 35S::TCP14/TCP15-GFP* plants. After immunoprecipitation of the extracts with an anti-GFP antibody, we detected both TCP14-GFP/TCP15-GFP and ULT1-FLAG in the same immunoprecipitate (Figure 2E and 2F). Thus, ULT1 indeed interacts with the TCP14/15 proteins in *Arabidopsis*. However, Y2H and LCI assay results showed that ULT1 does not interact with other class I TCP family members, such as TCP7 and TCP21 (Supplemental Figure 3).

The ULT1 protein contains an N-terminal putative DNA-binding SAND domain as well as a C-terminal B-box-like domain that may mediate protein–protein interactions (Carles et al., 2005). To explore which of these domains mediates the interaction with the TCP TFs, ULT1 was divided into an N-terminal region containing the conserved SAND domain and a C-terminal region containing the B-box-like domain (Supplemental Figure 4) for use in LCI assays. *N. benthamiana* leaves co-infiltrated with cLUC-TCP14/15 and nLUC-ULT1-C displayed strong interaction activity, whereas no LUC signal was detected in leaves co-infiltrated with cLUC-TCP14/15 and nLUC-ULT1-N (Figure 2G and 2H). These assays indicate that ULT1 interacts with TCP14/15 through its C-terminal domain.

ULT1 acts together with TCP14 and TCP15 to regulate organ size

To dissect the function of *TCP14/15* in the developmental process, we analyzed the expression patterns of *TCP14/15* in *Arabidopsis* and found that both *TCP14* and *TCP15* were highly expressed in rosette leaves (Supplemental Figure 5A and 5B). TCP14/15 are known to regulate *Arabidopsis* cell and organ growth, although *tcp14 tcp15* rosette leaves are reportedly the same size as WT rosette leaves (Peng et al., 2015). We therefore speculated that ULT1 and TCP14/15 might function in a common genetic pathway to regulate organ size. To test this hypothesis, we generated *ult1 tcp14 tcp15* triple-mutant plants

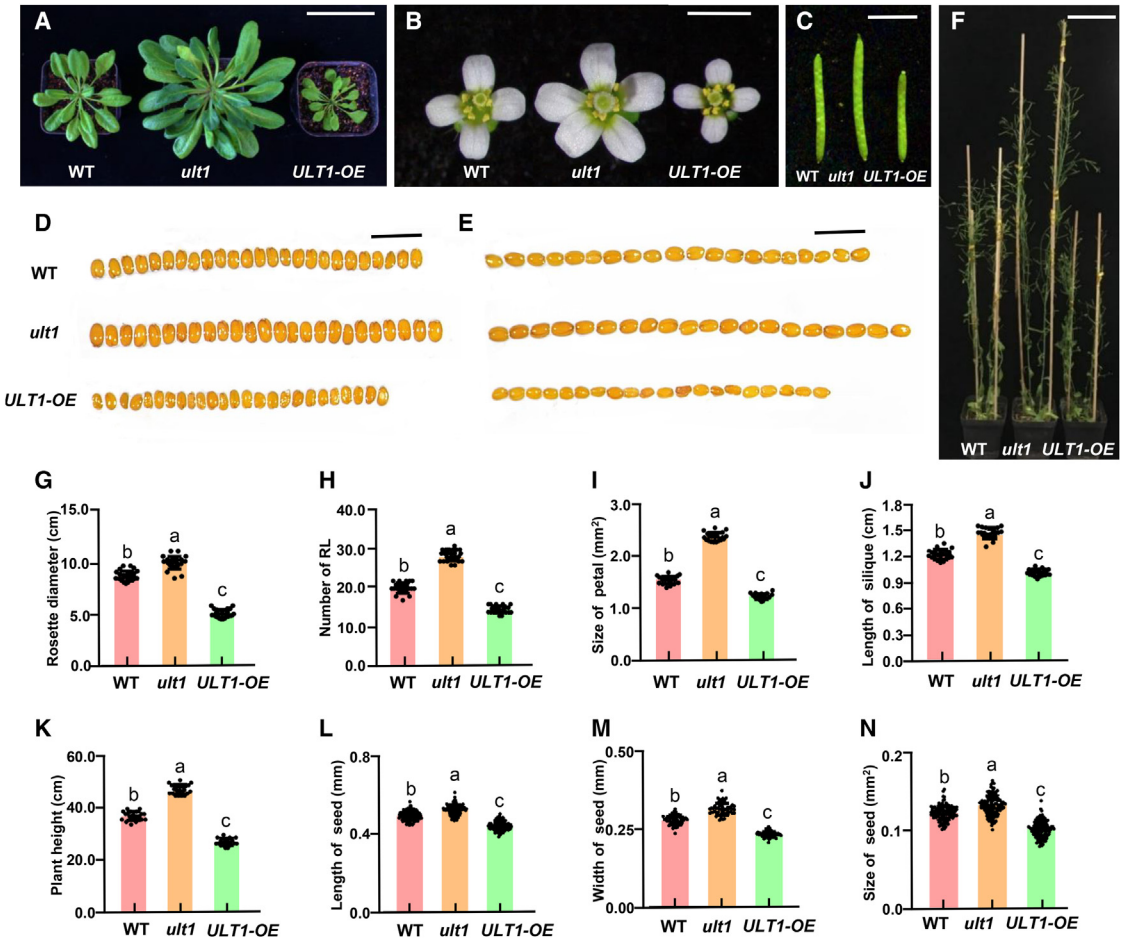

Figure 1. *ULT1* regulates plant organ size.

(A) Phenotypes of 40-day-old WT, *ult1*, and *35S::ULT1* transgenic plants (*ULT1-OE*). Scale bar, 6.5 cm.

(B) Flowers of WT, *ult1*, and *ULT1-OE* plants. Scale bar, 2 mm.

(C) Siliques of WT, *ult1*, and *ULT1-OE* plants. Scale bar, 4 mm.

(D) Seeds of WT, *ult1*, and *ULT1-OE* plants. Scale bar, 1.2 mm.

(E) Seeds of WT, *ult1*, and *ULT1-OE* plants placed end to end. Scale bar, 1.4 mm.

(F) Mature WT, *ult1*, and *ULT1-OE* plants. Scale bar, 6.5 cm.

(G) Rosette diameter of WT, *ult1*, and *ULT1-OE* plants. The values shown are means ± SE. Different letters represent significant differences determined by two-way ANOVA with Tukey's post hoc test ($p < 0.05$). n = 25.

(H) Rosette leaf numbers of WT, *ult1*, and *ULT1-OE* plants. The values shown are means ± SE. Different letters represent significant differences determined by two-way ANOVA with Tukey's post hoc test ($p < 0.05$). n = 25.

(I) Petal size of WT, *ult1*, and *ULT1-OE* plants. The values shown are means ± SE. Different letters represent significant differences determined by two-way ANOVA with Tukey's post hoc test ($p < 0.05$). n = 20.

(J) Silique length of WT, *ult1*, and *ULT1-OE* plants. The values shown are means ± SE. Different letters represent significant differences determined by two-way ANOVA with Tukey's post hoc test ($p < 0.05$). n = 20.

(K) Height of WT, *ult1*, and *ULT1-OE* plants. The values shown are means ± SE. Different letters represent significant differences determined by two-way ANOVA with Tukey's post hoc test ($p < 0.05$). n = 20.

(L) Seed length of WT, *ult1*, and *ULT1-OE* plants. The values shown are means ± SE. Different letters represent significant differences determined by two-way ANOVA with Tukey's post hoc test ($p < 0.05$). n = 120.

(M) Seed width of WT, *ult1*, and *ULT1-OE* plants. The values shown are means ± SE. Different letters represent significant differences determined by two-way ANOVA with Tukey's post hoc test ($p < 0.05$). n = 120.

(N) Seed size of WT, *ult1*, and *ULT1-OE* plants. The values shown are means ± SE. Different letters represent significant differences determined by two-way ANOVA with Tukey's post hoc test ($p < 0.05$). n = 120.

and compared their organ size phenotypes with those of WT, *ult1*, and *tcp14 tcp15* plants. Under our growth conditions, both *ult1* and *tcp14 tcp15* plants were larger than WT plants, and the phenotypes of *ult1 tcp14 tcp15* plants resembled those of *ult1* plants (Figure 3A–3E). The *ult1*, *tcp14 tcp15*, and *ult1 tcp14 tcp15* plants all formed larger rosettes and rosette leaves than WT plants (Figure 3A and 3C), and the sixth rosette leaves of *ult1*, *tcp14 tcp15*, and *ult1 tcp14 tcp15* plants were larger than those of WT plants (Figure 3B). Overall flower size was also greater in *ult1*, *tcp14 tcp15*, and *ult1 tcp14 tcp15* plants than in WT plants (Figure 3D). Likewise, *ult1*, *tcp14 tcp15*, and *ult1 tcp14 tcp15* plants all formed larger seeds than WT plants

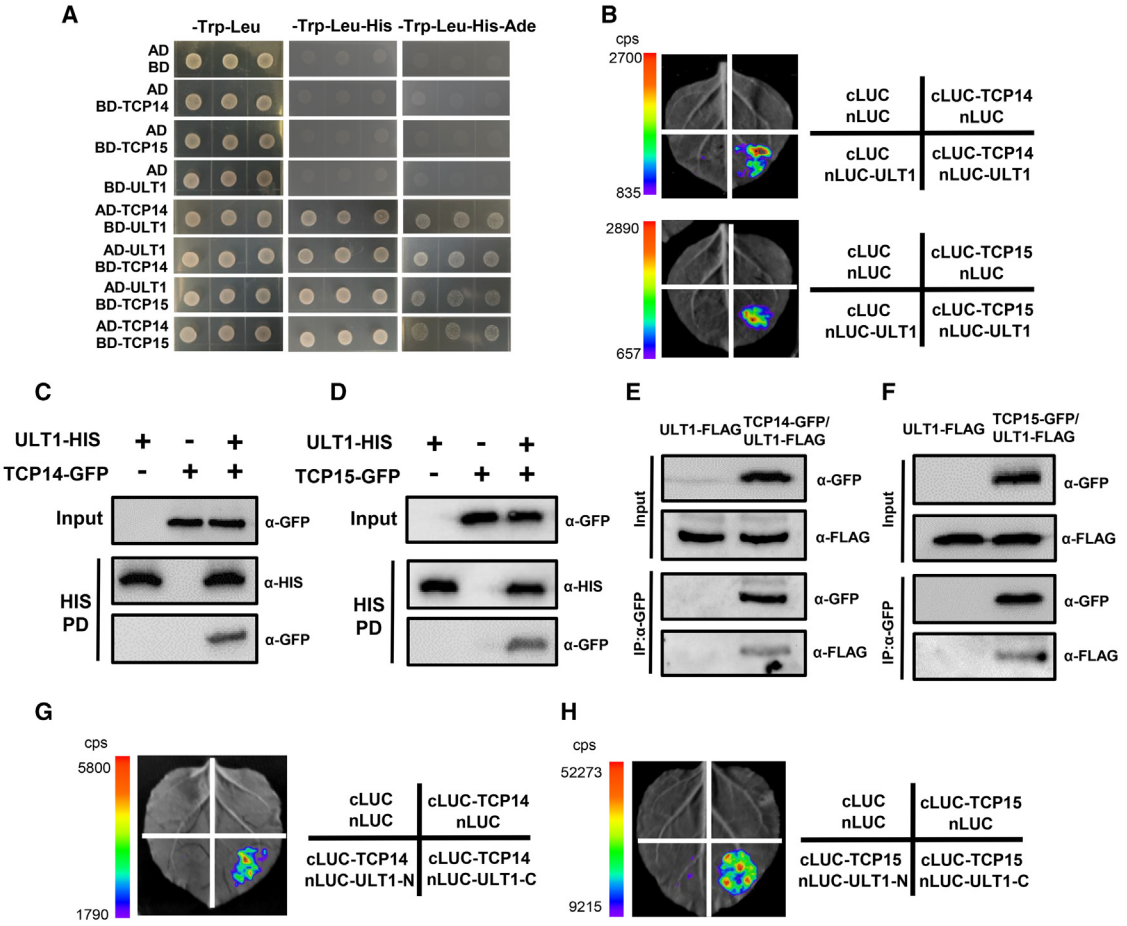

Figure 2. ULT1 physically interacts with TCP14 and TCP15 through the C-terminal region of ULT1.

(A) Yeast two-hybrid (Y2H) assays showing interactions between ULT1 and TCP14, ULT1 and TCP15, and TCP14 and TCP15. AD/BD, AD/BD-TCP14, AD/BD-TCP15, AD/BD-ULT1, AD-ULT1/BD-TCP14, AD-TCP14/BD-ULT1, AD-ULT1/BD-TCP15, and AD-TCP14/BD-TCP15 constructs were co-transformed into the AH109 yeast strain in pairwise combinations. Transformed yeast cells were selected on synthetic dextrose medium lacking Leu and Trp (−Trp/−Leu) and then transferred to synthetic dextrose medium lacking Leu, Trp, and His (−Trp/−Leu/−His) to assay for protein–protein interactions. The interactions were confirmed on synthetic dextrose medium lacking Leu, Trp, His, and Ade (−Trp/−Leu/−His/−Ade).

(B) Luciferase (LUC) complementation imaging (LCI) assays showing that ULT1 interacts independently with TCP14 and TCP15 in *N. benthamiana* leaves.

(C) Pull-down assays using ULT1-His and TCP14-GFP, showing that ULT1 interacts with TCP14.

(D) Pull-down assays using ULT1-His and TCP15-GFP, showing that ULT1 interacts with TCP15.

(E) Co-immunoprecipitation (coIP) of ULT1 and TCP14 proteins in *Arabidopsis* seedlings.

(F) CoIP of ULT1 and TCP15 proteins in *Arabidopsis* seedlings.

(G) LCI assays showing that the ULT1 C terminus interacts with TCP14 in *N. benthamiana* leaves.

(H) LCI assays showing that the ULT1 C terminus interacts with TCP15 in *N. benthamiana* leaves.

(Figure 3E). To quantify these phenotypes, we measured rosette diameter, sixth rosette leaf size, petal length, petal width, silique length, seed length, seed width, cotyledon size, petal size, and seed size; all of these organ size metrics were significantly greater in *ult1*, *tcp14 tcp15*, and *ult1 tcp14 tcp15* plants than in WT plants (Figure 3F–3K; Supplemental Figure 6E–6I). However, the *ult1 tcp14 tcp15* organ-size phenotype was not additive; instead, all the triple-mutant organs were similar to or just slightly smaller than the *ult1* organs, with both WT and *tcp14 tcp15* plants forming significantly smaller organs than the other two genotypes (Figure 3F–3K and Supplemental Figure 6E–6I). Thus, based on a previously-defined criterion for genetic interaction (i.e., that the double mutant phenotype can be considered epistatic when it resembles the phenotype of one of the single mutants) (Perez-Perez et al., 2009), these results suggest that ULT1 acts in the same genetic pathway with TCP14 and TCP15 to negatively control organ size in plants.

Cell proliferation and cell growth/expansion coordinately determine final organ size during plant organogenesis (Fleming, 2006; Breuer et al., 2010). To reveal the cellular mechanism by which ULT1 functions with TCP14/15 to control leaf size, we examined palisade and epidermal cell size as well as cell number in the sixth rosette leaves of WT, *ult1*, *tcp14 tcp15*, and *ult1 tcp14 tcp15* plants (Figure 4A). Both palisade and epidermal cells of *ult1*, *tcp14 tcp15*, and *ult1 tcp14 tcp15* leaves were dramatically larger than those of WT leaves (Figure 4B and 4C and Supplemental Figure 6J and 6K). The average area of palisade cells in *ult1*, *tcp14 tcp15*, and *ult1 tcp14 tcp15* 6th leaves was increased by 104.1%, 20.1%, and

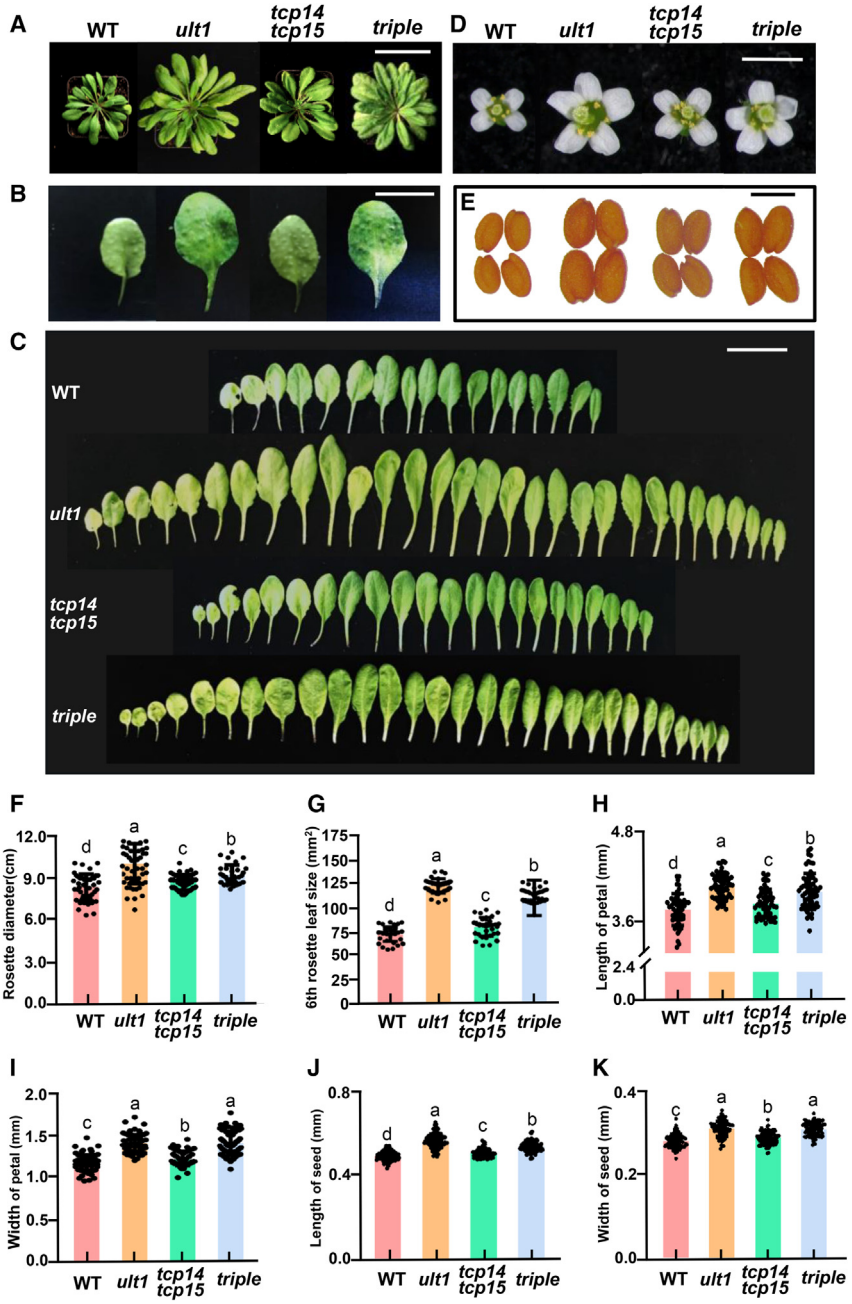

Figure 3. ULT1 acts together with TCP14/15 to regulate organ size in *Arabidopsis*.

(A) Phenotypes of 50-day-old WT, *ult1*, *tcp14 tcp15*, and *ult1 tcp14 tcp15* plants from left to right. Scale bar, 6.5 cm.

(B) The 6th rosette leaves of 40-day-old WT, *ult1*, *tcp14 tcp15*, and *ult1 tcp14 tcp15* plants from left to right. Scale bar, 1 cm.

(C) Rosette leaves of 50-day-old WT, *ult1*, *tcp14 tcp15*, and *ult1 tcp14 tcp15* plants from top to bottom. Scale bar, 2 cm.

(D) Flowers of WT, *ult1*, *tcp14 tcp15*, and *ult1 tcp14 tcp15* plants from left to right. Scale bar, 2 mm.

(E) Seeds of WT, *ult1*, *tcp14 tcp15*, and *ult1 tcp14 tcp15* plants from left to right. Scale bar, 0.5 mm.

(F) Rosette diameter of 50-day-old WT, *ult1*, *tcp14 tcp15*, and *ult1 tcp14 tcp15* plants. The values shown are means ± SE. Different letters represent significant differences determined by two-way ANOVA with Tukey's post hoc test ($p < 0.05$). n = 50.

(G) Sixth rosette leaf size of 40-day-old WT, *ult1*, *tcp14 tcp15*, and *ult1 tcp14 tcp15* plants. The values shown are means ± SE. Different letters represent significant differences determined by two-way ANOVA with Tukey's post hoc test ($p < 0.05$). n = 40.

(H) Petal length of WT, *ult1*, *tcp14 tcp15*, and *ult1 tcp14 tcp15* plants. The values shown are means ± SE. Different letters represent significant differences determined by two-way ANOVA with Tukey's post hoc test ($p < 0.05$). n = 60.

(I) Petal width of WT, *ult1*, *tcp14 tcp15*, and *ult1 tcp14 tcp15* plants. The values shown are means ± SE. Different letters represent significant differences determined by two-way ANOVA with Tukey's post hoc test ($p < 0.05$). n = 60.

(J) Seed length of WT, *ult1*, *tcp14 tcp15*, and *ult1 tcp14 tcp15* plants. The values shown are means ± SE. Different letters represent significant differences determined by two-way ANOVA with Tukey's post hoc test ($p < 0.05$). n = 100.

(K) Seed width of WT, *ult1*, *tcp14 tcp15*, and *ult1 tcp14 tcp15* plants. The values shown are means ± S.E. Different letters represent significant differences determined by two-way ANOVA with Tukey's post hoc test ($p < 0.05$). n = 100.

47.7%, respectively, compared with that of the WT (Figure 4B). By contrast, cell number was not significantly lower in these mutants than in WT plants (Supplemental Figure 6J and 6K), indicating that ULT1 and TCP14/15 mainly affect cell size. Hence, the larger size of *ult1*, *tcp14 tcp15*, and *ult1 tcp14 tcp15* rosette leaves results mainly from an increase in cell size, indicating that ULT1 acts with TCP14/15 to regulate *Arabidopsis* organ size by limiting cell expansion.

Cell size is frequently correlated with DNA ploidy levels in plants (Sugimoto-Shirasu and Roberts, 2003; Peng et al., 2015; Liu et al., 2019). To investigate whether the enlargement of cells in the mutant leaves was associated with an increase in DNA ploidy, we performed flow cytometry of nuclei from the sixth leaves of WT, *ult1*, *tcp14 tcp15*, and *ult1 tcp14 tcp15* plants. We quantified the relative proportions of cells in the 2C, 4C, 8C, 16C, and 32C states and found that endoreduplication levels were higher in *ult1*, *tcp14 tcp15*, and *ult1 tcp14 tcp15* leaves than in WT leaves, with endoreduplication levels of *ult1 tcp14 tcp15* leaves falling between those of *ult1* and *tcp14 tcp15* leaves (Figure 4D and 4E). High DNA ploidy was also observed in *tcp14 tcp15* compared with WT leaf nuclei, consistent with previous reports that TCP14 and TCP15 act redundantly to activate repressors of endoreduplication and suppress the endocycle process (Li et al., 2012; Peng et al., 2015). We next used endoreduplication index (EI), an indicator of cell endoreduplication level (Kocova et al., 2016; Bainard et al., 2020), to assess the endocycle level of WT and mutant leaves. Consistent with the larger cell size of the

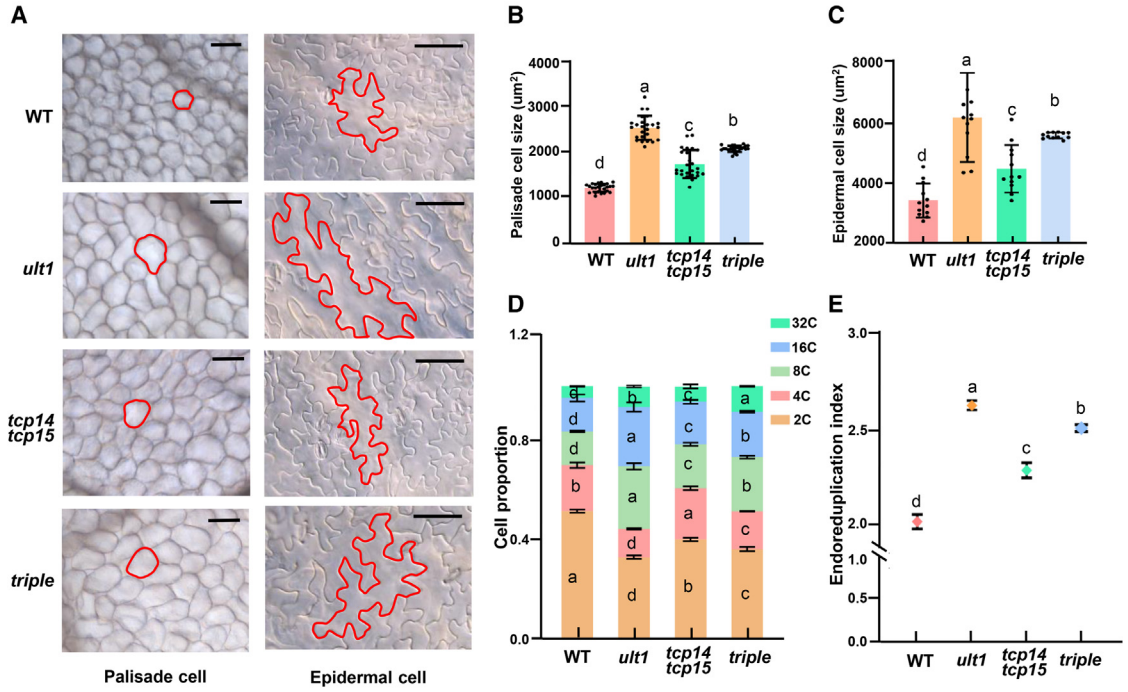

Figure 4. ULT1 acts together with TCP14/15 to regulate cell size by influencing cell endoreduplication.

(A) Palisade cells (left) and epidermal cells (right) in the sixth rosette leaf of WT, *ult1*, *tcp14 tcp15*, and *ult1 tcp14 tcp15* plants. Scale bar, 100 μm.

(B) Palisade cell size in the sixth rosette leaf of WT, *ult1*, *tcp14 tcp15*, and *ult1 tcp14 tcp15* plants. The values given are means (n = 60) ± SE. Different letters represent significant differences determined by two-way ANOVA with Tukey's post hoc test ($p < 0.05$).

(C) Epidermal cell size in the sixth rosette leaf of WT, *ult1*, *tcp14 tcp15*, and *ult1 tcp14 tcp15* plants. The values given are means (n = 15) ± SE. Different letters represent significant differences determined by two-way ANOVA with Tukey's post hoc test ($p < 0.05$).

(D) Nuclear DNA ploidy distribution of the sixth rosette leaf of WT, *ult1*, *tcp14 tcp15*, and *ult1 tcp14 tcp15* plants. The values represent averages of four independent biological replicates. Different letters represent significant differences determined by two-way ANOVA with Tukey's post hoc test ($p < 0.05$).

(E) Endoreduplication index (EI) of the sixth rosette leaf of WT, *ult1*, *tcp14 tcp15*, and *ult1 tcp14 tcp15* plants. The values represent averages of four independent biological replicates. Different letters represent significant differences determined by two-way ANOVA with Tukey's post hoc test ($p < 0.05$).

mutant leaves, *ult1*, *tcp14 tcp15*, and *ult1 tcp14 tcp15* leaves had higher EI levels than WT leaves (Figure 4E). These results indicate that ULT1 and TCP14/15 co-regulate endoreduplication and cell size during leaf growth in *Arabidopsis*.

ULT1 and TCP14/15 regulate common downstream genes involved in endoreduplication and leaf development

To further explore the molecular mechanism by which ULT1 and TCP14/15 regulate organ size, we performed high-throughput sequencing of total mRNA (RNA sequencing [RNA-seq]) from the rosette leaves of WT, *ult1*, and *tcp14 tcp15* plants. Correlation coefficients close to 1.0 for all of the tested samples indicated the high reproducibility of the experiments (Supplemental Figure 7A). Genes with at least a 2-fold expression change and an adjusted p value of less than 0.05 in *ult1* and *tcp14 tcp15* compared with WT plants were defined as differentially expressed genes (DEGs) (Supplemental Figure 7B and 7C). A total of 4766 DEGs were identified in *ult1* plants, 2660 (55.8%) of which were upregulated and 2106 (44.2%) of which were downregulated (Supplemental Figure 7D). A total of 6163 DEGs were identified in *tcp14 tcp15* plants, including 3304 (53.6%) upregulated and 2859 (46.4%) downregulated (Supplemental Figure 7D). The majority of DEGs, 3486 (73.1% and 56.6% relative to the total number of DEGs in *ult1* and *tcp14 tcp15* plants, respectively), were common downstream genes co-regulated by ULT1 and TCP14/15 (Figure 5A and Supplemental Figure 7D). Among these shared direct and indirect target genes, 56.8% were upregulated and 42.8% were downregulated in both *ult1* and *tcp14 tcp15* plants (Figure 5A and Supplemental Figure 7D and 7E). These transcriptome data show that ULT1 and TCP14/15 co-regulate a large set of common genes expressed in *Arabidopsis* rosette leaves.

Gene Ontology (GO) analysis showed that the common DEGs in *ult1* and *tcp14 tcp15* plants were enriched in 708 functional categories with a significant p value of less than 0.05; these included cell cycle, cell division, regulation of growth, and leaf development, as well as response to stress, protein ubiquitination, regulation of gene expression, and other functional categories (Supplemental Figure 8A; Supplemental Table 1). Expression patterns of representative genes enriched in the cell cycle, cell division, cell growth, and leaf development GO categories were visualized as heatmaps (Figure 5B and Supplemental Figure 8B). Interestingly, the majority of genes in these four categories were downregulated in *ult1* or *tcp14 tcp15* mutants (Figure 5B and Supplemental Figure 8B), consistent with previous evidence that ULT1 acts as a trxG factor to activate gene expression (Carles and Fletcher, 2009).

To confirm the RNA-seq results, the RNA transcripts of selected genes related to the cell cycle, cell division, and leaf development

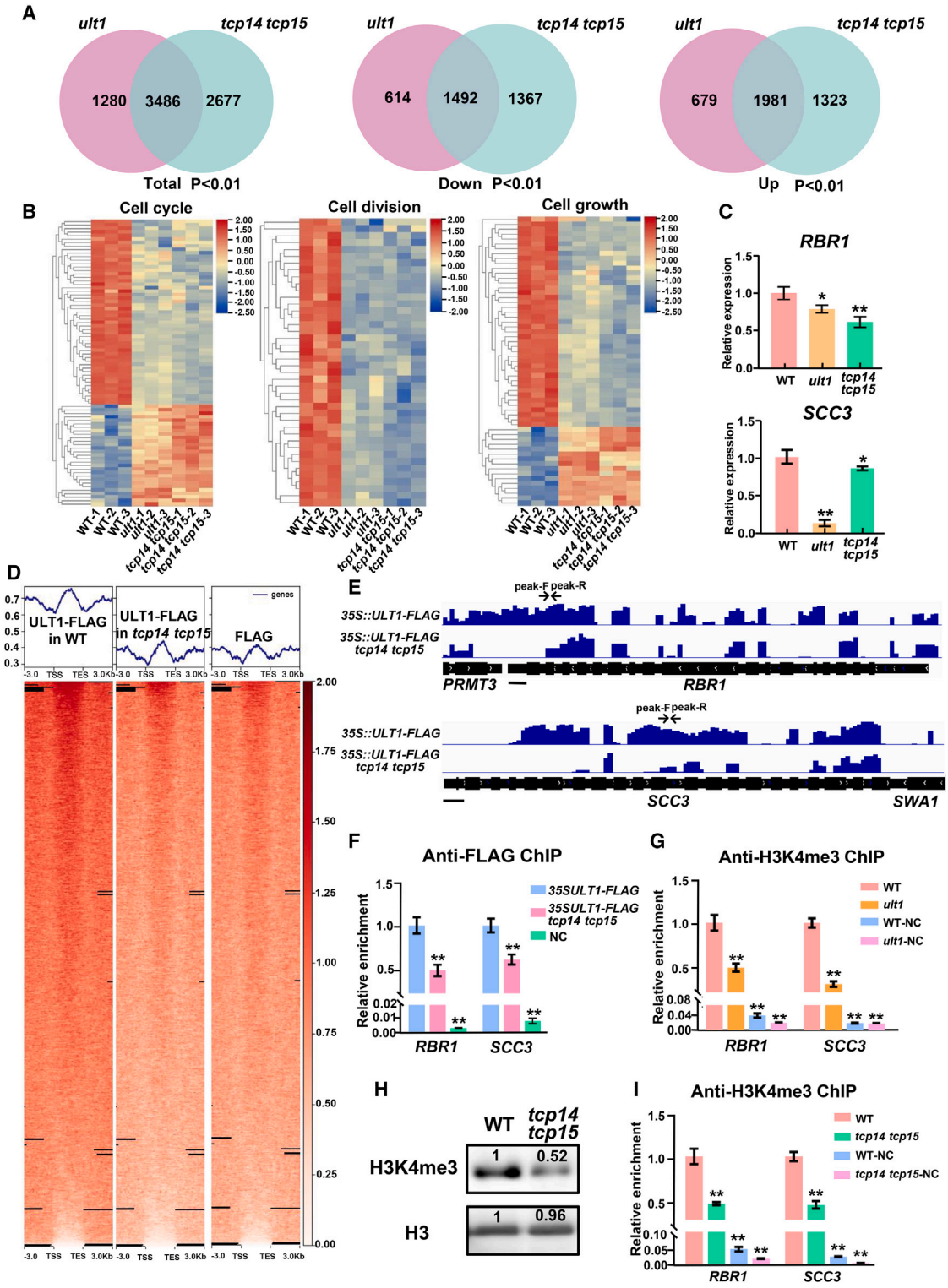

Figure 5. ULT1 is recruited to endoreduplication-related genes through TCP14/15 to deposit H3K4me3 to regulate target gene expression.

(A) Venn diagram of overlapping genes among differentially expressed genes (DEGs) in *ult1* and *tcp14 tcp15* plants. Total, total number of DEGs; up, upregulated DEGs; down, downregulated DEGs. The significance of the Venn diagram overlap is $p < 0.01$ as determined by Fisher's exact test.

(B) Heatmaps illustrating changes in the transcript levels of cell-cycle-related (left), cell-division-related (center), and cell-growth-related (right) genes of DEGs in *ult1* and *tcp14 tcp15* plants.

(legend continued on next page)

were examined by RT–qPCR (Figure 5C and Supplemental Figure 9A). Consistent with the RNA-seq data, the mRNA levels of genes that negatively regulate endoreduplication, such as *RBR1*, *GENERAL TRANSCRIPTION FACTOR GROUP E4*, *SISTER-CHROMATID COHESION PROTEIN 3* (*SCC3*), and *MEDIATOR OF RNA POLYMERASE II TRANSCRIPTION SUBUNIT 14*, were downregulated in *ult1* and *tcp14 tcp15* mutants compared with WT plants (Figure 5C; Supplemental Figure 9A). By contrast, four genes that promote endoreduplication, *KIP-RELATED PROTEIN 1*, *SMR7*, *SMR9*, and *ANAPHASE-PROMOTING COMPLEX SUBUNIT 13*, were upregulated in *ult1* and *tcp14 tcp15* plants (Supplemental Figure 9A). In addition, expression of the cell division-related gene *AUXIN RESPONSE FACTOR 9* was downregulated, whereas that of the leaf development gene *GRF3* was upregulated in *ult1* and *tcp14 tcp15* plants (Supplemental Figure 9A). Two other plant organ growth-related genes, *BB* and *PHYTOSULFOKINE 3* (*PSK3*), were also upregulated in *ult1* and *tcp14 tcp15* plants (Supplemental Figure 9A). To verify the correspondence between the RNA-seq and qPCR data, we calculated the log dCt change values of selected genes as reported previously (Jiang et al., 2018). The results showed that the expression levels determined by RT–qPCR and RNA-seq analysis were highly correlated (Supplemental Figure 9B and 9C), indicating that the independent methods produced consistent results. Together, these results indicate that ULT1 and TCP14/15 co-regulate a set of common target genes involved in endoreduplication and leaf development, in particular by inducing the transcription of genes that inhibit endoreduplication and repressing the transcription of genes that promote endoreduplication.

ULT1 is recruited to target loci by TCP14/15 to promote H3K4me3 deposition and activate gene expression

The finding that ULT1 and TCP14/15 co-regulate many common downstream genes led us to explore how they regulate the transcription of their targets. Previous studies have shown that ULT1 can bind target genes via its DNA-binding SAND domain (Xu et al., 2018a; Roy et al., 2019). We therefore investigated genome-wide ULT1 binding to target genes by performing a ChIP sequencing (ChIP-seq) experiment using *35S::ULT1-FLAG* plants and identified 4520 genes bound by ULT1 (Supplemental Table 2). We plotted the average binding signal across the upstream/downstream (6-kb) region surrounding the transcription start site (TSS) and the transcription end site (TES) and found that ULT1 was enriched in gene bodies (Figure 5D). GO analysis showed that ULT1-bound genes were enriched in functional categories such as regulation of gene expression, mitotic spindle organization, regulation of mitotic spindle assembly, unidimensional cell growth, anisotropic growth, and others (Supplemental Figure 10; Supplemental Table 3).

Because ULT1 acts as a trxG factor that can facilitate deposition of H3K4me3 marks, we next performed an H3K4me3 ChIP-seq analysis of WT and *ult1* plants to determine whether ULT1 influences genome-wide H3K4me3 enrichment. We identified 15 721 H3K4me3-marked genes in WT plants, which largely coincided with the H3K4me3-marked genes (76.6%) identified in a previous study (Zhang et al., 2009). We plotted the average binding signal across the upstream/downstream (6-kb) region surrounding the TSS and the TES and found that the overall H3K4me3 level was reduced in *ult1* compared with WT plants (Supplemental Figure 11A and 11B), suggesting that ULT1 is involved in H3K4me3 enrichment. To investigate whether ULT1 enrichment at its target genes is associated with H3K4me3 deposition, we determined the proportion of genes bound by ULT1 (ULT1-bound) that were also H3K4me3 marked in WT plants. Among the 4520 ULT1-bound genes, 2926 (64.7%) were marked by H3K4me3 ($p < 2.95 \times 10^{-29}$) (Supplemental Figure 12A; Supplemental Table 4), indicating that ULT1 mainly regulates target gene expression by binding to target loci and facilitating H3K4me3 modification.

To further investigate whether the DEGs shared by *ult1* and *tcp14 tcp15* are direct targets of ULT1, we combined our RNA-seq and ULT1 binding data and determined that 565 of 3486 genes ($p < 0.018$) co-regulated by ULT1 and TCP14/15 were directly bound by ULT1 protein (Supplemental Figure 12B; Supplemental Table 5). Notably, 62.3% (2173 of 3486) of the common DEGs and 78.2% (442 of 565) of the ULT1-bound common DEGs were marked by H3K4me3 (Supplemental Figure 12C; Supplemental Table 4), demonstrating that ULT1 association with TCP14/15 is required for H3K4me3 deposition at ULT1-bound loci. Similarly, when we analyzed the proportion of DEGs marked

(C) *RBR1* and *SCC3* mRNA levels in WT, *ult1*, and *tcp14 tcp15* rosette leaves. Graphs show relative expression levels normalized to that of the *ACTIN2* reference gene. qPCR was performed on at least four independent biological replicates. Error bars represent SD. *$p < 0.05$, **$p < 0.01$ by repeated-measures one-way ANOVA.

(D) Heatmap and metagene plots of ChIP-seq data from *35S::ULT1-FLAG*, *35S::ULT1-FLAG tcp14 tcp15*, and non-transgenic plants, showing the mean ULT1 enrichment signal at all ULT1 binding regions.

(E) ChIP-seq analysis of ULT1 binding at the *RBR1* and *SCC3* gene loci in *35S::ULT1-FLAG* and *35S::ULT1-FLAG tcp14 tcp15* plants. Gene models shown at the bottom include 5′ UTR (medium black line), exons (black boxes), introns (thin black line), and 3′ UTR (medium black line). The black line under the gene model represents a 250-bp scale. The double arrowheads above each gene model indicate the regions amplified for the ChIP–qPCR analysis.

(F) ChIP–qPCR analysis of ULT1 binding at *RBR1* and *SCC3* in *35S::ULT1-FLAG* and *35S::ULT1-FLAG tcp14 tcp15*. The anti-FLAG non-transgenic plant samples are a negative control (NC). ChIP–qPCR was performed on at least four independent biological replicates. Error bars represent SD. **$p < 0.01$ by repeated-measures one-way ANOVA.

(G) ChIP–qPCR analysis of H3K4me3 levels at the *RBR1* and *SCC3* loci in WT and *ult1* plants. Target gene loci without H3K4me3 enrichment were selected as NCs. ChIP–qPCR was performed on at least four independent biological replicates. Error bars represent SD. **$p < 0.01$ by repeated-measures one-way ANOVA.

(H) Global H3K4me3 levels in WT and *tcp14 tcp15* plants as determined by immunoblotting using an H3K4me3 antibody. The membrane was blotted with anti-H3 to confirm equal loading. The numbers on the bands show the protein levels relative to that of the WT, which was set to 1.

(I) ChIP–qPCR analysis of H3K4me3 levels at *RBR1* and *SCC3* in WT and *tcp14 tcp15* plants. Target gene loci without H3K4me3 enrichment were selected as NCs. ChIP–qPCR was performed on at least four independent biological replicates. Error bars represent SD. **$p < 0.01$ by repeated-measures one-way ANOVA.

by H3K4me3 in the individual *ult1* and *tcp14 tcp15* mutants, the overlap reached 61.3% (2920 of 4766, $p < 1.48 \times 10^{-10}$) and 62.4% (3844 of 6163, $p < 1.16 \times 10^{-20}$), respectively (Supplemental Figure 12D; Supplemental Table 4). GO analysis showed that the 565 ULT1-bound common DEGs were enriched in functional categories related to cell division, regulation of unidimensional cell growth, developmental growth, regulation of gene expression, response to water deprivation, protein ubiquitination, and other functional categories, with significant p values of less than 0.05 (Supplemental Figure 12E; Supplemental Table 6). Combined, these results demonstrate that TCP14/15 facilitate the ability of ULT1 to increase H3K4me3 marks on target loci, thereby regulating organ size in *Arabidopsis*.

To determine whether the recruitment of ULT1 to target genes is directly dependent on TCP14 and TCP15, *35S::ULT1-FLAG* plants were crossed into the *tcp14 tcp15* background to generate *35S::ULT1-FLAG tcp14 tcp15* plants. RT–qPCR confirmed that *ULT1* was expressed at high levels in these transgenic lines (Supplemental Figure 13A). We next performed ChIP-seq on *35S::ULT1-FLAG* and *35S::ULT1-FLAG tcp14 tcp15* plants to compare binding levels of ULT1 with its target gene loci in the presence and absence of TCP14/15. We plotted the average binding signal across the upstream/downstream (6-kb) region surrounding the TSS and the TES and found that ULT1 binding was reduced in *35S::ULT1-FLAG tcp14 tcp15* compared with *35S::ULT1-FLAG* (Figure 5D). Our analysis showed that, among the 4520 ULT1-bound genes, 2288 genes displayed decreased ULT1 enrichment in *35S::ULT1-FLAG tcp14 tcp15* plants compared with *35S::ULT1-FLAG* plants (Supplemental Table 7). GO analysis of the 2288 ULT1-bound but decreased genes (TCP14/TCP15-dependent genes) showed that these genes were significantly enriched in unidimensional cell growth, plant organ development, regulation of leaf development, regulation of growth and developmental growth, flower development, regulation of gene expression, and other functional categories (Supplemental Figure 14; Supplemental Table 8). Among 2288 TCP14/TCP15-dependent genes and 442 H3K4me3-marked ULT1-bound common DEGs, 230 were identified as TCP14/TCP15-dependent H3K4me3-marked and ULT1-bound common DEGs (Supplemental Table 9). GO analysis of these 230 genes showed that they were also enriched in the functional categories of cell division, DNA replication-dependent nucleosome assembly, regulation of unidimensional cell growth, developmental growth, regulation of developmental process, regulation of gene expression, protein ubiquitination, and others (Supplemental Figure 15; Supplemental Table 10). Among the 230 TCP14/TCP15-dependent H3K4me3-marked and ULT1-bound common DEGs, 72.6% (167) were downregulated in both *ult1* and *tcp14tcp15*, suggesting that these genes were regulated by TCP14/TCP15 and ULT1 via H3K4me3 modification (Supplemental Table 11). ChIP-seq analysis of *35S::ULT1-FLAG* and *35S::ULT1-FLAG tcp14 tcp15* plants suggested that ULT1 occupation was reduced in *35S::ULT1-FLAG tcp14 tcp15* compared with *35S::ULT1-FLAG* at the target genes *RBR1* and *SCC3* (Figure 5E), which affect endoreduplication and cell size and showed reduced expression levels in *ult1* mutants (Figure 5C). ChIP–qPCR analysis of ULT1 binding at these two loci in *tcp14 tcp15* plants confirmed that these genes had lower ULT1 occupancy levels in the absence of *TCP14/15* (Figure 5F), indicating that loss of *TCP14* and *TCP15* impairs the recruitment of ULT1 to target genes.

To investigate the effects of ULT1 on TCP14/TCP15 binding to target genes, we generated *35S::TCP14/TCP15-MYC* and *35S::TCP14/TCP15-MYC ult1* plants. RT–qPCR confirmed that *TCP14* and *TCP15* were expressed at high levels in these transgenic lines (Supplemental Figure 13B and 13C). We performed ChIP-seq to analyze TCP14 and TCP15 enrichment at their target loci in *35S::TCP14/TCP15-MYC* and *35S::TCP14/TCP15-MYC ult1* plants. We plotted the average binding signal across the upstream/downstream (6-kb) region surrounding the TSS and the TES and found that the overall TCP14/TCP15 enrichment signals of *35S::TCP14/TCP15-MYC ult1* were indistinguishable from those of *35S::TCP14/TCP15-MYC* (Supplemental Figure 16A and 16B). ChIP-seq and ChIP–qPCR analysis confirmed that enrichment of TCP14 and TCP15 on the target genes in the *ult1* background was not significantly different from that in the WT background (Supplemental Figure 16C–16F). These results indicate that binding of TCP14/TCP15 to their target genes is not influenced by *ULT1* mutation. We then analyzed H3K4me3 patterns at the *RBR1* and *SCC3* loci in WT and *ult1* plants using ChIP-seq and ChIP–qPCR. Both sets of results demonstrated that H3K4me3 levels on the two target genes were lower in *ult1* than in WT plants (Figure 5G; Supplemental Figure 11D and 11E), consistent with their reduced transcript levels in the *ult1* background (Figure 5C).

To further confirm that TCP14/15 recruit ULT1 to target loci to promote H3K4me3 deposition, we assessed global H3K4me3 levels by western blotting and found that H3K4me3 enrichment was reduced by half (48%) in *tcp14 tcp15* compared with WT plants (Figure 5H). We then performed H3K4me3 ChIP-seq of WT and *tcp14 tcp15* mutants and plotted the average binding signal across the upstream/downstream (6-kb) region surrounding the TSS and the TES. Consistent with previous results, the overall H3K4me3 level was markedly reduced in *tcp14 tcp15* plants compared with the WT (Supplemental Figure 11A and 11C), indicating that TCP14/15 are required to facilitate genome-wide H3K4me3 deposition. To confirm the ChIP-seq results, we examined levels of H3K4me3 enrichment at the *RBR1* and *SCC3* loci in WT and *tcp14 tcp15* plants and found that loss of *TCP14/TCP15* indeed reduced H3K4me3 levels at the two target genes compared with those in the WT (Figure 5I). In addition, we analyzed H3K4me3 levels in *35S::TCP14/TCP15-MYC* and *tcp14 tcp15* plants using ChIP-seq and plotted the average binding signal across the upstream/downstream (6-kb) region surrounding the TSS and the TES. We found that the overall H3K4me3 level was lower in *tcp14 tcp15 mutants* than in *35S::TCP14* and *35S::TCP15-MYC* transgenic plants (Supplemental Figure 17A and 17B). H3K4me3 enrichment at the target genes *RBR1* and *SCC3* was also reduced (Supplemental Figure 17C and 17D), consistent with the overall reduction in H3K4me3 levels in *tcp14 tcp15* compared with *35S::TCP14/TCP15-MYC* plants. Taken together, these results indicate that TCP14 and TCP15 recruit the trxG protein ULT1 to promote H3K4me3 deposition and enhance expression of endoreduplication- and cell-size-related target genes such as *RBR1* and *SCC3*,

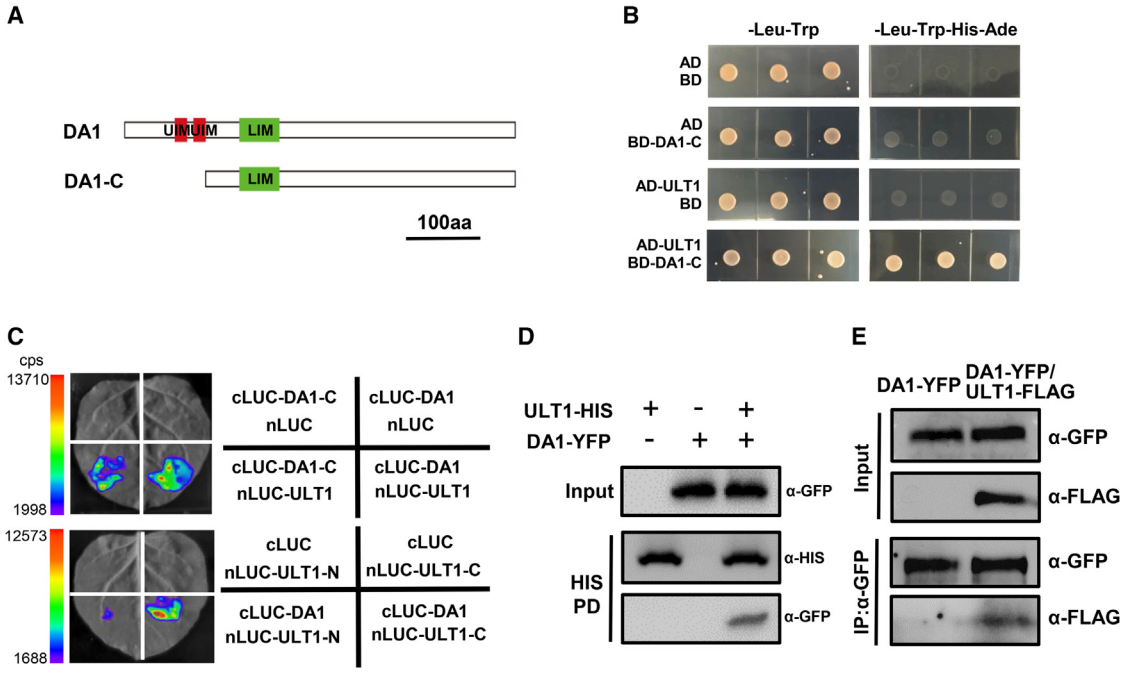

Figure 6. ULT1 physically interacts with DA1 through the C-terminal region of ULT1.

(A) Schematic of full-length DA1 protein containing a pair of ubiquitin interaction motifs (UIMs) and an LIM domain and its truncation into DA1-C, which lacks the self-activating UIM domains.

(B) Y2H analysis showing interaction between ULT1 and DA1-C.

(C) LCI assays showing interactions between ULT1 and DA1-C, ULT1 and DA1, and ULT1-C and DA1 in *N. benthamiana* leaves.

(D) Pull-down assays of ULT1 and DA1 proteins showing that ULT1 interacts with DA1.

(E) CoIP assay of ULT1 and DA1 proteins in *Arabidopsis* seedlings.

thus influencing cell size and determining final organ size in *Arabidopsis*.

ULT1 influences the interaction between DA1 and TCP14/15 to antagonize the effect of DA1 on TCP14/TCP15 degradation

DA1 regulates endoreduplication by physically associating with TCP14 and TCP15 proteins and causing their degradation (Peng et al., 2015; Dong et al., 2017). Because ULT1 also interacts with TCP14/15 to regulate cell size, we hypothesized that DA1 might interact with ULT1 in organ size control. To investigate the relationship between ULT1 and DA1, we first performed Y2H assays with the ULT1 and DA1 proteins. Because the full-length DA1 sequence, especially the ubiquitin interaction motif (UIM) domain, can autoactivate in DNA-BD fusion vectors (Dong et al., 2017), we generated a truncated version called DA1-C that contained only the LIM domain and the C-terminal region (Figure 6A). The results showed that DA1-C could interact with ULT1 in yeast cells (Figure 6B). We next performed LCI assays in which DA1-C or full-length DA1 was fused to cLUC and ULT1 was fused to nLUC to generate the DA1-C-cLUC, DA1-cLUC, and ULT1-nLUC constructs. Strong interaction activity was detected when either DA1-C-cLUC and ULT1-nLUC or DA1-cLUC and ULT1-nLUC were co-expressed in *N. benthamiana* leaves (Figure 6C). Because we found that ULT1 interacts with TCP14/15 through its C-terminal region, we then tested whether ULT1 interacts with DA1 through the same region. When DA1-cLUC and ULT1-N-nLUC or DA1-cLUC and ULT1-C-nLUC were co-expressed in *N. benthamiana* leaves, an interaction was observed only between DA1-cLUC and ULT1-C-nLUC (Figure 6C), indicating that ULT1 physically interacts with DA1 as well as with TCP14/15 through its C-terminal domain. Pull-down assays to detect ULT1-His purified protein in *35S::DA1-YFP* plants also demonstrated that ULT1 interacts with DA1 (Figure 6D). Finally, coIP assays were performed to confirm the interaction *in vivo* using *35S::DA1-YFP* and *35S::DA1-YFP 35S::ULT1-FLAG* transgenic plants. We detected both ULT1-FLAG and DA1-YFP proteins in *35S::DA1-YFP 35S::ULT1-FLAG* extracts but only DA1-YFP proteins in *35S::DA1-YFP* extracts (Figure 6E), demonstrating that DA1 indeed interacts with ULT1 in *Arabidopsis*.

On the basis of evidence that ULT1 physically associates with both DA1 and TCP14/15 via its C-terminal domain and that DA1 also associates with TCP14/15 (Peng et al., 2015; Dong et al., 2017), we asked whether either ULT1 or DA1 influences the other's interaction with TCP14/15 and whether DA1 affects the role of the ULT1–TCP14/15 module in organ size control. We first performed a yeast three-hybrid (Y3H) assay to explore the effect of DA1 on the interaction between ULT1 and TCP14/15. This assay showed that ULT1 strongly interacted with TCP14 and TCP15 in the absence of DA1-C, whereas the interaction between ULT1 and TCP14/15 was drastically reduced in the presence of DA1-C (Supplemental Figure 19), suggesting that DA1 might compete with ULT1 for interaction with TCP14/15. To further examine the possible competition of DA1 with ULT1 for interaction with TCP14/15, we performed LCI assays in *N. benthamiana* leaves combined with western blotting. The results showed that the

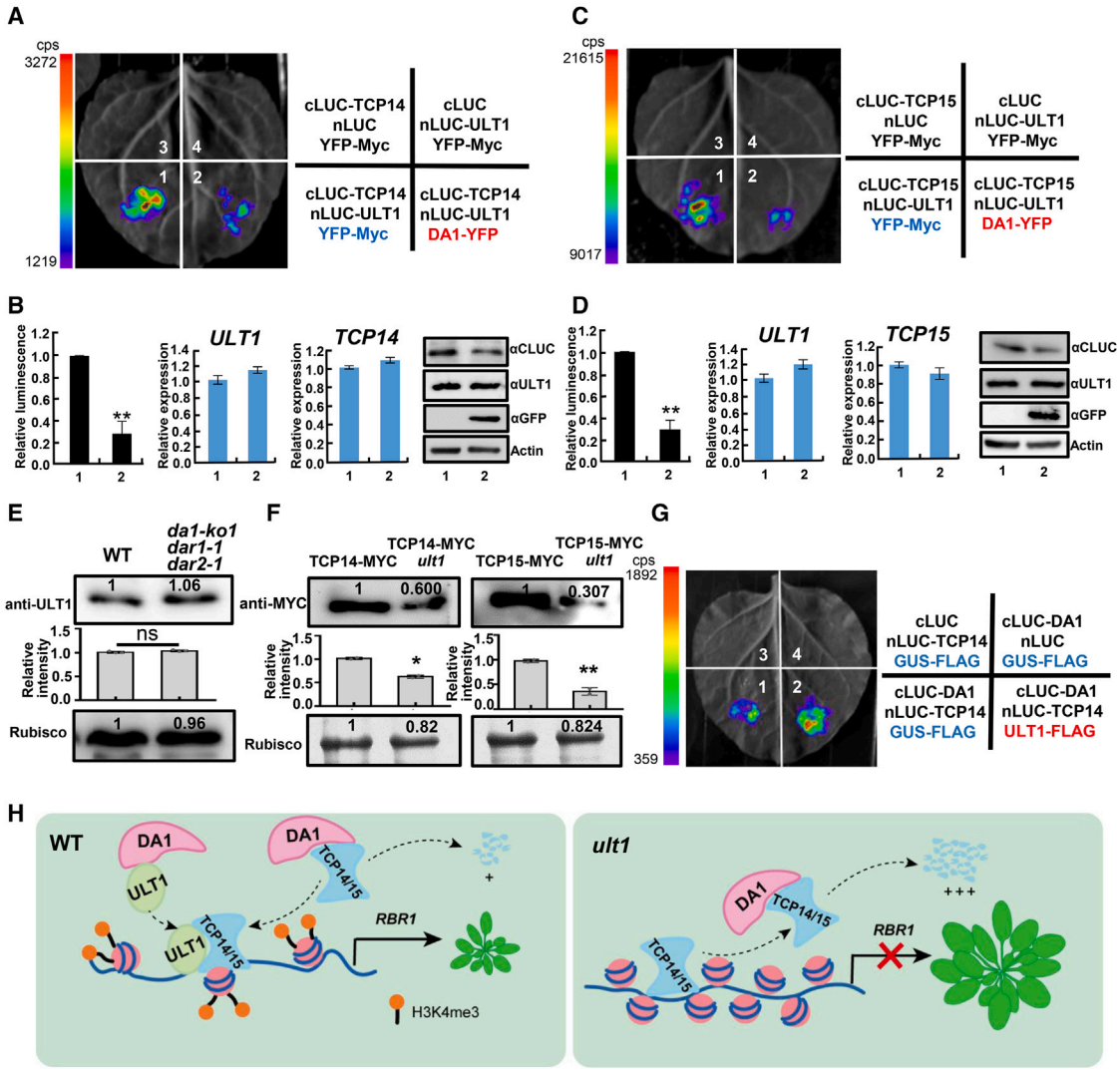

Figure 7. DA1 interferes with the interaction of ULT1 and TCP14/15.

(A) LCI assays of the effect of DA1 on the interaction between ULT1 and TCP14. Region 1 is the section of the *N. benthamiana* leaf co-transformed with cLUC-TCP14, nLUC-ULT1, and YFP-MYC lacking DA1. Region 2 is the section co-transformed with cLUC-TCP14, nLUC-ULT1, and DA1-YFP. Region 3 is the section co-transformed with cLUC-TCP15, nLUC, and YFP-MYC. Region 4 is the section co-transformed with cLUC, nLUC-ULT1, and YFP-MYC. Regions 3 and 4 served as NCs. The experiment was independently replicated five times.

(B) Relative fluorescence signals, *ULT1* and *TCP14* transcript levels, and TCP14, ULT1, and DA1 protein levels in regions 1 and 2 of the *N. benthamiana* leaf in **(A)**. n = 5, **p < 0.01 by repeated-measures one-way ANOVA.

(C) LCI assays of the competitive interference of DA1 with the interaction between ULT1 and TCP15. Region 1 is the section of the *N. benthamiana* leaf co-transformed with cLUC-TCP15, nLUC-ULT1, and YFP-MYC lacking DA1. Region 2 is the section co-transformed with cLUC-TCP15, nLUC-ULT1, and DA1-YFP. Region 3 is the section co-transformed with cLUC-TCP15, nLUC, and YFP-MYC. Region 4 is the section co-transformed with cLUC, nLUC-ULT1, and YFP-MYC. Regions 3 and 4 served as NCs. The experiment was independently replicated five times.

(D) Relative fluorescence signals, *ULT1* and *TCP15* transcript levels, and TCP15, ULT1, and DA1 protein levels in regions 1 and 2 of the *N. benthamiana* leaf in **(C)**. n = 5, **p < 0.01 by repeated-measures one-way ANOVA.

(E) ULT1 protein accumulation in WT and *da1-ko1 dar1-1 dar2-1* plants, quantified by ImageJ software. The numbers on the bands show the relative protein levels, with that of the WT set to 1. The experiment was independently replicated three times. ns, not significant by repeated-measures one-way ANOVA.

(F) TCP14/15-MYC protein accumulation in WT and *ult1* plants, quantified by ImageJ software. The experiment was independently replicated three times. *p < 0.05, **p < 0.01 by repeated-measures one-way ANOVA.

(G) LCI assays showing the relative strength of the interaction between cLUC-DA1 and nLUC-TCP14 in the absence or presence of ULT1-FLAG. The experiment was independently replicated four times.

(H) A proposed model for the regulation of rosette leaf size by ULT1, TCP14/15, and DA1 in *Arabidopsis*. In WT plants, ULT1 is recruited to target genes by interacting with TCP14/15 and promotes the deposition of active H3K4me3 marks at the target loci. ULT1 and DA1 influence each other's interactions

(legend continued on next page)

ULT1–TCP14/15 interaction was eliminated in the presence of excess DA1 (Figure 7A and 7C), but *TCP14/15* and *ULT1* transcript levels were unchanged, regardless of whether DA1 was present or absent (Figure 7B and 7D). Western blotting showed that TCP14-LUC and TCP15-LUC protein levels were not significantly altered in the presence of ULT1 (Figure 7B and 7D), whereas these protein levels were drastically reduced in the absence of ULT1 (Supplemental Figure 21D). These data confirmed that the decreased interaction signals in the TCP14/15 and ULT1 system were not due to reduced TCP14/15 protein levels but rather to the competition between ULT1 and DA1 for binding to TCP14/15. In addition, we performed LCI assays in which cLUC-DA1-C and nLUC-TCP14 or cLUC-ULT1 and nLUC-TCP14 were co-expressed in *N. benthamiana* leaves to investigate the relative strength of the interactions between the ULT1-TCP and DA1-TCP proteins. As measured by relative fluorescence intensity, the strength of the ULT1–TCP14 interaction was not significantly different from that of the DA1–TCP interaction (Supplemental Figure 18). Collectively, these results demonstrate that DA1 can influence the physical interaction of ULT1 with the TCP14/15 TFs.

Because the interaction between DA1 and the TCP14/15 proteins results in degradation of the two TFs (Peng et al., 2015; Dong et al., 2017), we hypothesized that the association of DA1 with ULT1 might lead to its degradation as well, resulting in reduced interaction between ULT1 and TCP14/15 in the presence of DA1. A straightforward test of this hypothesis is that if DA1 and/or its related proteins DA1-RELATED PROTEIN 1 (DAR1) and DAR2 can degrade ULT1, then ULT1 protein levels will be increased in loss-of-function *da1-ko1 dar1-1 dar2-1* triple-mutant plants. However, we found that ULT1 protein levels were unchanged in *da1-ko1 dar1-1 dar2-1* plants compared with WT plants (Figure 7E). In addition, we quantified ULT1 protein levels in a DA1 competition experiment in *N. benthamiana* leaves (Figure 7A and 7C) and found that ULT1 remained unchanged when DA1 protein was added, suggesting that ULT1 protein is not degraded by DA1 (Figure 7B and 7D). We also compared ULT1 protein levels in *35S::ULT1-FLAG* and *35S::ULT1-FLAG 35S::DA1-YFP* transgenic plants and detected no change in ULT1 protein levels in the presence of high levels of DA1 (Supplemental Figure 20A). Finally, we co-expressed ULT1-FLAG and DA1-YFP fusion proteins in *N. benthamiana* leaves and quantified ULT1 protein levels by western blotting. These results also showed that DA1 does not influence ULT1 protein accumulation (Supplemental Figure 20D and 20E). Taken together, these results indicate that DA1 is not involved in degradation of ULT1 protein and that neither DA1 nor its related proteins affect the stability of ULT1 in *Arabidopsis*. Therefore, the reduced interaction signals we observed between TCP14/15 and ULT1 in the presence of DA1 in yeast and *N. benthamiana* leaf cells might be caused by competition between DA1 and ULT1 for interaction with TCP14/15.

We next assessed whether ULT1, like DA1, influences TCP14/15 protein accumulation. We first compared TCP14/15 protein levels in *35S::TCP14/15-MYC* versus *35S::TCP14/15-MYC ult1* plants by western blotting. TCP14/15 protein levels were reduced when *ULT1* was functionally impaired (Figure 7F), suggesting that ULT1 positively regulates TCP14/15 protein accumulation. We also compared TCP14/TCP15 protein levels in *35S::TCP14/TCP15-GFP* versus *35S::ULT1-FLAG 35S::TCP14/TCP15-GFP* transgenic plants and found that *ULT1* OE significantly increased TCP14/TCP15 protein levels (Supplemental Figure 20B and 20C). To further verify the relationship among these three proteins, we expressed TCP14/TCP15-MYC, ULT1-FLAG, and DA1-YFP fusion proteins in *N. benthamiana* leaves and quantified the protein levels of TCP14/TCP15 and ULT1. The results confirmed that the addition of DA1 decreased TCP14/TCP15 protein accumulation, but the presence of ULT1 compromised the degradation of TCP14/TCP15 by DA1 (Supplemental Figure 20D and 20E). We next tested the effect of ULT1 on the interaction between DA1 and TCP14 using LCI assays. The strength of the signal produced by the interaction between DA1 and TCP14 was enhanced in the presence of ULT1 (Figure 7G; Supplemental Figure 21A), although ULT1 did not affect the expression levels of either *DA1* or *TCP14* (Supplemental Figure 21B and 21C). Finally, we quantified TCP14 protein levels in regions 1 and 2 of the co-transformed *N. benthamiana* leaf in Figure 7G and found that addition of ULT1 indeed increased TCP14 protein accumulation (Supplemental Figure 21D). Together, these data are consistent with a scenario in which ULT1 prevents DA1 from accessing the TCP14 protein and inducing its degradation.

Although ULT1 and DA1 interact with TCP14/15, all proteins in this module are involved in the transcriptional regulation of target gene expression. We therefore examined whether their interaction occurs in the nucleus. We first investigated the subcellular localization of ULT1 and DA1 proteins by transforming *35S::ULT1-GFP* and *35S::DA1-YFP* fusion constructs accompanied by the nuclear localization marker *AHL22* into *N. benthamiana* leaves. ULT1 and DA1 proteins displayed similar subcellular localization patterns, with fluorescence signals accumulating mainly in the nuclei (Supplemental Figure 22A), suggesting that both proteins are localized in the nucleus, consistent with previous reports (Monfared et al., 2013; Vanhaeren et al., 2020). We then performed bimolecular fluorescence complementation assays in which ULT1 was fused to nonfluorescent N-terminal YFP (YN-ULT1) and DA1 was fused to C-terminal YFP (YC-DA1). The results confirmed that the interaction between ULT1 and DA1 indeed occurs in the nucleus (Supplemental Figure 22B). Together, our data demonstrate that the plant-specific trxG protein ULT1 and the LIM peptidase DA1 play crucial but antagonistic roles in the regulation of TCP14/15 activity, providing significant insights into the epigenetic mechanisms underlying regulation of organ size in *Arabidopsis*.

DISCUSSION

How organ size is regulated is a fundamental question in developmental biology, but the genetic and molecular mechanisms that determine organ size are still unclear. In this study, we report that

with TCP14/15, weakening the association between DA1 and TCP14/15. These interactions result in reduced degradation of TCP14/15 by DA1, allowing the TFs to activate expression of endoreduplication- and cell-growth-related genes such as *RBR1* and thus negatively regulate endoreduplication, which is required for normal cell size and leaf size in *Arabidopsis*. In *ult1* plants, H3K4me3 marks on target genes are reduced, and DA1 degrades more TCP14/15 protein in the absence of ULT1, inhibiting expression of endoreduplication- and cell-growth-related genes. This results in an increase in endoreduplication, leading to an increase in cell size and overall rosette leaf size in plants.

the plant-specific trxG protein, ULT1, is recruited to target genes by the TFs TCP14/15 and then promotes H3K4me3 deposition and activates expression of endoreduplication- and leaf development-related genes. We demonstrate that ULT1 associated with TCP14/15 regulates cell size through endoreduplication, thereby determining organ size in *Arabidopsis*. Furthermore, DA1 can antagonize ULT1 for binding to TCP14/15 and interferes with the interaction between ULT1 and TCP14/15. These findings provide significant insights into the epigenetic regulatory mechanisms that link regulation of cell and organ size to endoreduplication in *Arabidopsis*.

TrxG proteins control gene transcription and regulate development through the modification of chromatin within the nucleus (Schuettengruber et al., 2017). Previous reports have described ULT1 as a putative transcriptional regulator involved in root, shoot, and floral meristem maintenance and floral meristem determinacy. Our ChIP-seq results show that many ULT1-bound genes are highly enriched in the categories of shoot system development and flower development (Supplemental Figure 10), further confirming the indispensable function of ULT1 in shoot and floral meristem development. However, epigenetic regulators of organ size control have not been identified to date. Here, we reveal a novel function for ULT1 in the regulation of vegetative and reproductive organ size. Loss of *ULT1* function resulted in overall larger plant phenotypes, including more and larger rosette leaves, bigger siliques and seeds, and taller plants, whereas transgenic plants overexpressing *ULT1* displayed smaller organ phenotypes than WT plants (Figure 1A–1F and Supplemental Figure 1C–1F). These results demonstrate that ULT1 is necessary and sufficient to negatively regulate the size of almost all organs in *Arabidopsis* plants. In addition, our results showed that ULT1 mainly affected cell size but also slightly affected cell number (Figure 4A–4C and Supplemental Figure 6J and 6K). Organ development is the result of coordinated events of cell division and expansion in strong interaction with each other. As development proceeds, the proliferative activity of cells progressively slows, and the transition from cell division to expansion phases is accompanied by repeated endoreduplication for cell enlargement and final cell size (Bertin, 2005; Gonzalez et al., 2012). Thus, our data may suggest a possible compensation effect mechanism between cell division and expansion, mediated by ULT1. Nevertheless, because organ size is a key trait for crop breeding, it will be interesting to investigate the role of ULT1 in control of crop organ size and use its homologs to improve biomass in key agricultural species.

TrxG factors are epigenetic regulators that mediate the large-scale establishment and maintenance of active gene expression states. The trxG proteins, including ULT1, have been reported to function in various aspects of transcriptional activation by promoting the deposition of H3K4me3 activation marks (Kingston and Tamkun, 2014; Pu and Sung, 2015; Fletcher, 2017). The ability of trxG proteins to remodel chromatin and modify histones enables them to regulate the expression of thousands of genes (Kingston and Tamkun, 2014; Li et al., 2015). Despite the importance and conservation of the trxG machinery, the means by which it recognizes its target loci remain unclear. In *Drosophila*, PcG and trxG complexes can be recruited to PREs and trithorax response elements at target loci, thus driving the epigenetic inheritance of silent or active chromatin states throughout development (Kassis and Brown, 2013; Chetverina et al., 2017). Although PcG and trxG are highly conserved from flies to humans to plants, it is not yet clear to what extent their regulatory mechanisms are shared between plants and animals, and PREs or trithorax response elements have not fully been found as the docking sites of specific recruiters in plants. Instead, a diverse group of TFs and non-coding (ncRNA) appear to recruit PcG proteins to target genes in plants (Heo and Sung, 2011; Hecker et al., 2015; Li et al., 2016). By contrast, much less research has been performed to identify trxG recruiters. Nevertheless, the TFs LEAFY (LFY) and SEP3 have been reported to recruit SPLAYED (SYD)/BRAHMA (BRM), a trxG factor that is a member of the SWItch/Sucrose Non-Fermentable (SWI/SNF) family of chromatin remodelers, to activate target genes (Wu et al., 2012). Therefore, to elucidate the ULT1 targeting mechanism in *Arabidopsis*, we screened an *Arabidopsis* TF library and identified two TFs, TCP14 and TCP15, as ULT1 partner proteins (Figure 2). We then generated evidence indicating that TCP14/15 recruit ULT1 to promote H3K4me3 deposition at their target genes to promote their transcriptional activation. First, the ULT1-binding levels on 2288 of 4520 (50.6%) ULT1-bound loci significantly decreased in the absence of TCP14 and TCP15 (Figure 5D), including those on the endoreduplication-limiting target genes *RBR1* and *SCC3* (Figure 5E and 5F; Supplemental Table 7), demonstrating that the recruitment of ULT1 to target loci is dependent on TCP14/TCP15. Second, the DEGs identified in *tcp14 tcp15* plants showed high overlap with H3K4me3-marked genes (Supplemental Figure 12D), suggesting that TCP14/15-regulated genes are associated with H3K4me3 active marks. Third, overall H3K4me3 levels were lower in *tcp14 tcp15* plants than in the WT (Figure 5H), suggesting that TCP14/15 may facilitate H3K4me3 deposition for transcriptional activation on a large scale. Fourth, overall H3K4me3 enrichment in *ult1* and *tcp14 tcp15* plants was reduced compared with that in WT plants, including at the *RBR1* and *SCC3* loci (Supplemental Figure 11), suggesting that ULT1 association with TCP14/15 is required for robust H3K4me3 accumulation. In addition, *35S::TCP14-MYC* and *35S::TCP15-MYC* plants overexpressing *TCP14* and *TCP15* had higher overall H3K4me3 enrichment levels than *tcp14 tcp15* mutants (Supplemental Figure 17), further indicating that TCP14/TCP15 are associated with H3K4me3 methylation. All of these results suggest that these two TCP TFs act as recruiters to recruit the trxG protein ULT1 to target loci and promote H3K4 trimethylation to enhance transcriptional activity, which is consistent with the overall function of class I TCPs in growth promotion (Martin-Trillo and Cubas, 2010; Gastaldi et al., 2020). In summary, our data reveal a previously undescribed function of TCP14/15 as ULT1 recruiters to connect trxG-mediated epigenetic regulation and cell size in plants.

We demonstrated that ULT1 physically interacts with the plant-specific TCP14/15 TFs through its C-terminal region both *in vitro* and *in vivo* (Figure 2). TCP15 can directly bind to the promoters of cell-cycle- and endoreduplication-related genes, including *CYCA2;3* and *RBR1*, to promote their expression (Li et al., 2012). Endoreduplication positively contributes to cell size, and increased endoreduplication may lead to larger-than-normal cells and organs (Mizukami, 2001; Sugimoto-Shirasu and Roberts, 2003). TCP14 and TCP15 have been reported to act redundantly to control endoreduplication (Kieffer et al., 2011; Peng et al., 2015), suggesting that the interaction between ULT1 and the TCP14 and TCP15 proteins has functional significance. We investigated the genetic interaction between *ULT1* and *TCP14* and *TCP15* and

observed that, although *tcp14 tcp15* double mutants showed only a slight increase in organ size, the introduction of *ult1* into *tcp14 tcp15* plants resulted in enlarged organs, similar in size to those of *ult1* plants (Figure 3A–3K and Supplemental Figure 6A–6I). Consistent with these results, the *ult1 tcp14 tcp15* triple mutation influenced leaf size, leaf cell size, and leaf cell ploidy levels (Figure 4A–4E). Thus, our genetic analysis indicates that ULT1 acts with TCP14 and TCP15 to negatively control plant organ size. Transcriptome analysis showed that ULT1 and TCP14/15 share a set of common downstream target genes, including genes associated with endoreduplication and leaf development, further confirming that ULT1 associates with TCP14/15 in a common pathway to control organ size in *Arabidopsis* (Figure 5A and 5B and Supplemental Figures 7D, 7E, and 8).

We generated several lines of evidence indicating that the physical association of ULT1 with the TCP14/15 proteins affects the accumulation of the two TFs. First, TCP14/15 protein levels are reduced in *35S::TCP14/15-MYC ult1* plants compared with *35S::TCP14/15-MYC* plants (Figure 7F). OE of *ULT1* significantly increases TCP14/TCP15 protein levels (Supplemental Figure 20B and 20C). Third, transient expression assays in *N. benthamiana* leaves showed that the presence of DA1 reduces TCP14/TCP15 protein levels, whereas the presence of ULT1 increases them (Supplemental Figure 20D and 20E). Lastly, testing the effect of ULT1 on the interaction between DA1 and TCPs using LCI assays demonstrated that addition of ULT1 increases TCP14 protein accumulation (Supplemental Figure 21D). Taken together, these results indicate that ULT1 can increase TCP14/15 protein levels.

The LIM peptidase DA1 and its related proteins interact with TCP14/15 to control organ growth by influencing cell endoreduplication (Peng et al., 2015). DA1 has many functions, including facilitation of substrate degradation, and DA1 indeed degrades TCP14/15 proteins to influence endoreduplication in *Arabidopsis* (Dong et al., 2017). Considering the evidence that ULT1 enhances, but DA1 reduces, the relative abundance of TCP14/15 proteins, a plausible explanation would be that DA1 and ULT1 could influence each other's binding to the TCP proteins and thus affect the formation of functional ULT1–TCP14/15 protein complexes for H3K4me3 and expression activation of target loci. This notion is supported by our data. First, Y3H assays showed that ULT1 strongly interacts with TCP14 and TCP15 in the absence, but not the presence, of DA1-C (Supplemental Figure 19), suggesting that DA1 might compete with ULT1 for binding to TCP14/15. Second, LCI experiments showed that DA1 addition reduces the interaction between ULT1 and TCP14/15 (Figure 7A and 7C), whereas ULT1 addition increases the interaction between DA1 and TCP14/15 (Figure 7G and Supplemental Figure 21). TCP14/TCP15 protein levels do not change significantly in the presence of ULT1 (Figure 7B and 7D), suggesting that the reduced interaction between TCP14/15 and ULT1 is not due to reduced TCP14/15 protein levels but rather to possible competition between ULT1 and DA1 for binding to TCP14/15. Third, co-expression of the three fusion proteins TCP14/TCP15-MYC, ULT1-FLAG, and DA1-YFP in *N. benthamiana* leaves showed that DA1 addition reduced TCP14/TCP15 protein accumulation, whereas ULT1 addition compromised the degradation of TCP14/TCP15 by DA1 (Supplemental Figure 20D and 20E). Fourth, LCI assays showed that addition of ULT1 to the interaction system of DA1 and TCPs increased the interaction signals (Figure 7G and Supplemental Figure 21A), and western blotting revealed that addition of ULT1 increased TCP14 protein accumulation (Supplemental Figure 21D). Finally, we verified that the interaction occurs in the nucleus, where transcriptional regulation of target genes takes place (Supplemental Figure 22). Taken together, these results confirm that ULT1 and DA1 have crucial but antagonistic effects on TCP14/15 activity, thereby determining organ size in *Arabidopsis*.

On the basis of molecular, biochemical, and genetic evidence, we propose a possible working model for ULT1–TCP14/15–RBR1-mediated control of rosette leaf size in *Arabidopsis* (Figure 7H). In WT plants, ULT1 is recruited to target genes by interacting with TCP14/15 and promotes the deposition of H3K4me3 marks to activate transcription. ULT1 interacts with the LIM peptidase DA1 for binding to TCP14/15, which weakens the interaction between DA1 and TCP14/15. These interactions result in reduced degradation of TCP14/15 and increased expression of their endoreduplication- and plant organ growth-related target genes, such as *RBR1*, which is required for normal cell and organ size in *Arabidopsis*. In the absence of ULT1, H3K4me3 marks on target genes are reduced, and DA1 promotes more TCP14/15 degradation, thus inhibiting the expression of target genes such as *RBR1* that increase endoreduplication and increasing cell size and rosette leaf size in plants. However, it remains to be clarified how ULT1 influences TCP14/15 protein levels and potentially prevents the access of DA1 to TCPs. It is possible that ULT1 activation and DA1 degradation are both required for certain developmental aspects of *Arabidopsis*, depending on varying expression levels of ULT1 and DA1 in a particular context. Future studies are needed to determine how ULT1 antagonizes the degradation of TCP proteins by DA1 in a specific organ or at a certain developmental stage. Nevertheless, our findings define a novel epigenetic and molecular mechanism by which an ULT1–TCP14/15–RBR1 regulatory module might compete with the LIM peptidase DA1 to control organ size in *Arabidopsis*. Organ size, including seed size, is a key trait for crop breeding. It will be a challenge to investigate the functions of this epigenetic module in key crops and exploit their homologs and natural alleles to increase biomass and yield in the future.

METHODS

Plant materials and growth conditions

Arabidopsis WT, *ult1*, *tcp14-3 tcp15-3* (*tcp14 tcp15*), and *da1-ko1 dar1-1 dar2-1* used in this study were in the Columbia (Col-0) background. The *tcp14 tcp15* and *da1-ko1 dar1-1 dar2-1* mutants were kindly provided by Prof. Yunhai Li (Chinese Academy of Sciences). *ult1 tcp14 tcp15* triple mutants were generated by crossing *ult1* and *tcp14 tcp15* plants. *35S::ULT1-FLAG* transgenic plants were generated for phenotypic analysis, ChIP-seq, and coIP assays. The coding sequence (CDS) of *ULT1* was cloned and recombined into the *p1300-221* vector via the *Xba*I and *Sal*I restriction enzymes to generate the *35S::ULT1-FLAG* vector. The *35S::ULT1-FLAG* construct was introduced into the *Agrobacterium tumefaciens* strain GV3101, and the transgenic agrobacteria were transformed into Col-0 plants via the floral dip method (Clough and Bent, 1998) to generate *35S::ULT1-FLAG* transgenic plants. The *35S::TCP14-MYC* and *35S::TCP15-MYC* constructs were provided by Prof. Yunhai Li and introduced into WT plants. *35S::TCP14/TCP15-MYC* and *ult1* plants were crossed to generate *35S::TCP14/TCP15-MYC ult1* plants for analysis of TCP14/15 protein stability and ChIP-seq analysis of TCP14/15 binding.

The *35S::TCP14-GFP* and *35S::TCP15-GFP* constructs were introduced into *A. tumefaciens* strain GV3101, and the transgenic agrobacteria were transformed into *35S::ULT1-FLAG* plants via the floral dip method (Clough and Bent, 1998) to generate *35S::ULT1-FLAG 35S::TCP14-GFP* and *35S::ULT1-FLAG 35S::TCP15-GFP* plants for ULT1 and TCP14/TCP15 coIP assays. *35S::DA1-GFP* constructs were generated and transformed into WT and *35S::ULT1-FLAG* plants for ULT1 and DA1 coIP assays. *35S::ULT1-FLAG* and *tcp14 tcp15* plants were crossed to generate *35S::ULT1-FLAG tcp14 tcp15* plants for ChIP-seq and ChIP–qPCR analysis. All transformants were identified by screening on half-strength Murashige and Skoog medium containing 50 μg/ml Basta or 50 mg/l hygromycin. Eight to fifteen independent transgenic lines were obtained for each transformant. Seeds were collected from individual T1 plants. Selected T2 plants were propagated, and homozygous lines were confirmed by genotyping analysis. Homozygous T3 progeny were obtained for further analysis. All *Arabidopsis* seeds were surface sterilized and grown on agar plates containing half-strength Murashige and Skoog medium. The seeds were kept at 4°C for 2 days and moved to a short-day growth room (8-h light/16-h dark) at 21°C for 14 days. At this time, seedlings were considered to be 14 days after germination (DAG). Seedlings were then transferred to soil for growth under long-day conditions (16-h light/8-h dark) at 21°C in a greenhouse.

Morphological and cellular analyses

Flowers, rosette leaves, siliques, and seeds were photographed under a Leica M80 stereoscopic microscope to obtain digital pictures, and organ sizes (e.g., rosette diameter, rosette leaf size, petal length, petal width, petal size, silique length, seed length, seed width, and seed size) were measured using ImageJ software. The rosette diameter of each plant was defined as the longest distance between two leaves on opposite sides of the meristem; this metric is positively correlated with rosette area and used to describe variation in rosette growth, as reported previously (Adhikari et al., 2021; Wieters et al., 2021). To analyze cell size and cell number, the 6th rosette leaves were collected and fixed in destaining solution (75% ethanol and 25% acetic acid) until the chlorophyll was cleared. A basic solution (7% NaOH in 60% ethanol) was added for 20 min to soften and exfoliate the samples. The samples were then rehydrated in an ethanol gradient (60%, 40%, 20%, 10%) for 20 min and preserved in a solution of 25% glycerol in 5% ethanol. The cells were observed and photographed using differential interference contrast optics on a Leica microscope (DM2500). Cell size was measured as described in a previous report (Zhang et al., 2020). Cell number was calculated in longitudinal direction/length and transverse direction/width, as described previously (Xu et al., 2018b; Lyu et al., 2020; Hao et al., 2021).

For flow cytometry experiments, 50-day-old 6th rosette leaves were chopped with a razor blade in LB01 buffer (15 mM Tris, 2 mM EDTA, 0.5 mM spermine tetrahydrochloride, 80 mM KCl, 20 mM NaCl, and 0.1% Triton X-100) and filtered through a cell strainer with a 30-μm mesh. RNase A was added to a final concentration of 50 μg/ml, and the samples were stained with 50 μg/ml propidium iodide. Ploidy levels were measured using a flow cytometer (BD FACS Aria). At least 11 000 nuclei were used for each ploidy measurement. Flow cytometry experiments were repeated at least three times for each genotype using independent biological replicates.

Y2H assays

The *Arabidopsis* TF library was kindly provided by Prof. Lijia Qu (Peking University). The activating domain (AD) and binding domain (BD) constructs used for Y2H assays were generated in the *pGADT7* (Clontech) and *pGBKT7* (Clontech) vectors via homologous recombination. The full-length coding sequences of *ULT1*, *TCP14*, *TCP15*, *DA1*, and *DA1-C* were cloned into the *Eco*RI and *Bam*HI sites of the *pGADT7* vector to generate the *ULT1-AD*, *TCP14-AD*, *TCP15-AD*, *DA1-AD*, and *DA1-C-AD* constructs. Similarly, the full-length coding sequences of *ULT1*, *TCP14*, *TCP15*, *DA1*, and *DA1-C* were cloned into the *Eco*RI and *Pst*I sites of the *pGBKT7* vector to generate the *ULT1-BD*, *TCP14-BD*, *TCP15-BD*, *DA1-BD*, and *DA1-C-BD* constructs. The constructs were then co-transformed pairwise into the AH109 yeast strain. Transformed yeast cells were selected on synthetic dextrose medium lacking Leu and Trp (−Trp/−Leu) and then transferred to synthetic dextrose medium lacking Leu, Trp, and His (−Trp/−Leu/−His) to assay for protein–protein interactions. The interactions were confirmed on synthetic dextrose medium lacking Leu, Trp, His, and Ade (−Trp/−Leu/−His/−Ade). The assays were repeated at least three times for each interaction.

Y3H assays

The AD constructs used for Y3H were generated as described for the Y2H assays. To construct the *pBridge-ULT1-DA1-C* vector, the full-length coding sequence of *ULT1* was cloned into the *Eco*RI and *Bam*HI sites in the multiple cloning site I (MCS I) of the *pBridge* vector (Clontech) fused to the GAL4 DNA-binding domain, and the coding sequence of *DA1-C* was cloned into the MCS II site of the *pBridge* vector expressed as the "bridge" protein only in the absence of methionine. The *pBridge-ULT1* vector was used as a control without the "bridge" protein. The constructs were co-transformed into the AH109 yeast strain. The presence of the transgenes was confirmed by growth on synthetic dextrose/−Leu/−Trp plates. The same OD-value co-transformed yeast cells were spread on plates containing synthetic dextrose/−Leu/−Trp/−His medium or synthetic dextrose/−Leu/−Trp/−His/−Met medium, with or without the expression of the third protein. Each transformed yeast was serially diluted tenfold (1×, 10×, and 100×) and spotted onto dropout synthetic medium.

LCI assays

LCI assays were performed in *N. benthamiana* leaves as described previously (Liu et al., 2016). The full-length coding sequences of *ULT1*, *ULT1-N*, *ULT1-C*, *TCP14*, *TCP15*, *DA1*, and *DA1-C* were cloned into the *Kpn*I and *Sal*I sites of the *nLUC* vector to generate the *nLUC-ULT1*, *nLUC-ULT1-N*, *nLUC-ULT1-C*, *nLUC-TCP14*, *nLUC-TCP15*, *nLUC-DA1*, and *nLUC-DA1-C* constructs. The full-length coding sequences of *ULT1*, *ULT1-N*, *ULT1-C*, *TCP14*, *TCP15*, *DA1*, and *DA1-C* were cloned into the *Kpn*I and *Bam*HI sites of the *cLUC* vector to generate the *cLUC-ULT1*, *cLUC-ULT1-N*, *cLUC-ULT1-C*, *cLUC-TCP14*, *cLUC-TCP15*, *cLUC-DA1*, and *cLUC-DA1-C* constructs. *A. tumefaciens* strain GV3101 harboring nLUC- and cLUC-derived constructs were co-infiltrated into *N. benthamiana*, and the infiltrated leaves were analyzed for LUC activity 48 h after infiltration. LUC activity was measured using a NightSHADE LB 985 instrument (Berthold). The nLUC/cLUC combination was used as a negative control (NC). The experiment was repeated at least three times.

For competition experiments, *cLUC-TCP14*, *cLUC-TCP15*, and *nLUC-ULT1* were generated as described above, and the coding sequence of *DA1* was fused to GFP in the *pEarleyGate 101* vector to generate the competing protein construct (Earley et al., 2006). *35S::YFP-MYC* was expressed instead of DA1-YFP as an NC. Separately, *cLUC-DA1* and *nLUC-TCP14* were generated as described above, and the coding sequence of *ULT1* was fused to FLAG in the *p1300-221* vector to generate the competing protein construct. *35S::GUS-FLAG* was expressed instead of ULT1-FLAG as an NC. *N. benthamiana* leaves were infiltrated with agrobacteria carrying combinations of equal amount of three constructs, and LUC activity was measured using a NightSHADE LB 985 instrument (Berthold). The experiment was repeated at least three times.

For the interaction strength experiment, *cLUC-DA1-C* and *nLUC-TCP14* or *cLUC-ULT1* and *nLUC-TCP14* were generated as described above and co-infiltrated into the same *N. benthamiana* leaf. LUC activity was visualized using a NightSHADE LB 985 instrument (Berthold). The experiment was repeated at least three times.

Bimolecular fluorescence complementation assays

The full-length sequences of *ULT1* and *DA1* were cloned into the *pEarleyGate201-YN* and *pEarleyGate202-YC* vectors, respectively, to generate

the *YN-ULT1* and *YC-DA1* constructs. *YN-ULT1*, *YC-DA1*, and a nuclear localization marker, *RFP-AHL22* (Wang et al., 2013), were transformed into *A. tumefaciens* strain GV3101. *N. benthamiana* leaves were infiltrated with agrobacteria containing all three constructs. The combination of *YN* and *YC* was used as an NC. The leaves were imaged with a Zeiss LSM 700 laser-scanning confocal microscope.

In vivo pull-down assays

A full-length *ULT1* cDNA was amplified and inserted into the *pET28a* vector. The recombinant ULT1-His protein was expressed in *Escherichia coli* BL21 (DE3) (Transgen, CD701-01), then purified and immobilized on His-tag protein purification beads (Solarbio) according to the manufacturer's instructions. The beads were incubated with the TCP14/TCP15-GFP and DA1-YFP protein lysate for 3 h at 4°C. Supernatants were resolved by 12% SDS–PAGE and immunoblotted using anti-His and anti-GFP antibodies.

CoIP assays

CoIP experiments were performed as described previously (Dong et al., 2020). In brief, 14-day-old *35S::ULT1-FLAG* and *35S::ULT1-FLAG 35S::TCP14/TCP15/DA1-GFP/YFP* seedlings were collected, and their total proteins were extracted with lysis buffer (50 mM Tris–HCl [pH 7.5], 150 mM NaCl, 5 mM EDTA [pH 8.0], 0.1% Triton X-100, 0.2% NP-40, 1 nM freshly added PMSF, complete protease inhibitor cocktail [Roche], and 10 μM MG132). After centrifugation, protein A beads (Invitrogen) were incubated with the supernatant for 4 h, and anti-GFP antibody was then added and co-incubated overnight. The beads were washed three times with wash buffer (50 mM Tris–HCl [pH 7.5], 150 mM NaCl, 20% glycerol, 0.1% Triton X-100, 1 mM EDTA [pH 8.0], complete protease inhibitor cocktail [Roche], and 10 μM MG132). The immunoprecipitates were separated by 10% SDS–PAGE and detected by immunoblot analysis with anti-FLAG (Sigma) and anti-GFP (Abclonal) antibodies.

Subcellular localization analysis

The full-length *ULT1* coding sequence was cloned into the *pEarleyGate103* vector for fusion with a GFP protein to generate the *35S::ULT1-GFP* construct. The full-length *DA1* coding sequence was cloned into the *pEarleyGate101* vector for fusion with a YFP protein to generate the *35S::DA1-YFP* construct. These constructs, as well as that of the nuclear localization marker *RFP-AHL22*, were co-transformed into *A. tumefaciens* strain GV3101, and *N. benthamiana* leaves were infiltrated with pairwise sets of agrobacteria. The GFP, YFP, and RFP signals were observed and imaged using a Zeiss LSM 700 laser-scanning confocal microscope.

RNA-seq and RT–qPCR analysis

Mixed rosette leaves of 50-day-old WT, *ult1*, and *tcp14 tcp15* plants were collected, and total RNA was extracted with TRIzol reagent (Invitrogen) according to the manufacturer's instructions. Three independent biological replicates were used. cDNA libraries were generated and prepared for high-throughput Illumina sequencing. The RNA-seq reads were examined using FASTQC and then mapped to the reference genome of *Arabidopsis* using TopHat2. The mapping rates of all samples reached up to 95%. Genes that showed a greater than 2-fold expression change in the mutant were designated as up- or downregulated when the mutant RNA level was higher or lower than that of the WT, respectively ($|\log2$ [fold change]$| > 1$, adjusted $p < 0.05$).

For RT–qPCR analysis, the RNA samples were treated with DNase I to remove genomic DNA. First-strand cDNA was synthesized from 1 μg of total RNA via the SuperScript II reverse transcriptase kit (Invitrogen) according to the manufacturer's instructions. qPCR using SYBR Green PCR Master Mix (ABI) was performed on at least two independent biological replicates. *ACTIN2* was used as an internal control for data normalization.

ChIP and ChIP–qPCR assays

All ChIP experiments were performed using the Hyperactive Universal CUT&Tag Assay Kit for Illumina (Vazyme). About 10^5 cell nuclei from *35S::ULT1-FLAG* and *35S::ULT1-FLAG tcp14 tcp15* were extracted by the ChIP method as described previously (Xu et al., 2018a), and tagmentation genomic DNA was obtained according to the manufacturer's instructions. For library amplification, 15 μl of DNA was mixed with 25 μl 2× TruePrep Amplify mix and 5 μl of ddH_2O, as well as 5 μl of uniquely barcoded i5 and i7 primers from the TruePrep Index Kit V2 for Illumina (Vazyme). A total volume of 50 μl of sample was placed in a thermocycler for amplification using the following program: 72°C for 3 min; 95°C for 3 min; 12 cycles of 98°C for 10 s and 60°C for 5 s; 72°C for 1 min, and hold at 4°C. To purify the PCR products, 1.2× volumes of VAHTS DNA Clean Beads (Vazyme) were added and incubated at room temperature for 10 min. Libraries were washed twice with 80% ethanol and eluted in 22 μl of ddH_2O. Libraries were sequenced on the Illumina NovaSeq platform, and 150-bp paired-end reads were generated. qPCR using SYBR Green PCR Master Mix was performed to measure the enrichment of ULT1 protein on its target genes in *35S::ULT1-FLAG* transgenic plants in the presence or absence of TCP14/15.

For the anti-H3K4me3 ChIP experiment, total chromatin was extracted from 14-day-old WT, *ult1*, *tcp14 tcp15*, and *35S::TCP14/TCP15-MYC* seedlings and immunoprecipitated using an anti-H3K4me3 antibody (Sigma) as described above. qPCR using SYBR Green PCR Master Mix was performed to measure the enrichment of H3K4me3 on the target genes.

For the anti-MYC ChIP experiment, total chromatin was extracted from 14-day-old *35S::TCP14/TCP15-MYC* and *35S::TCP14/TCP15-MYC ult1* seedlings and immunoprecipitated using an anti-MYC antibody (Merck) as described above. qPCR using SYBR Green PCR Master Mix was performed to measure the enrichment of TCP14/TCP15 on the target genes.

The ULT1-specific antibody was generated by Beijing Enris Biotechnology for the ULT1 protein accumulation test.

Total histone protein blotting

Total histone proteins were extracted from WT and *tcp14 tcp15* plants using the EpiQuik Total Histone Extraction Kit (OP-0006-100) according to the manufacturer's instructions. The extracted histone proteins were used for protein blotting with the antibodies listed below. An anti-H3 immunoblot was used as a loading control. Antibodies were as follows: anti-H3 (ab1791, Abcam) and anti-H3K4me3 (07-473, Millipore).

Analysis of phylogeny, gene structure, and conserved domains

All full-length amino acid sequences were used for phylogenetic tree construction. All sequences were aligned using ClustalW. The phylogenetic trees were constructed using the neighbor-joining method in MEGA X with 500 bootstrap replications (Kumar et al., 2018). We chose the p-distance method for quantification of phylogenetic trees. The gene structures were visualized using Gene Structure Display Server v.2.0 (Guo et al., 2007). Domain analysis was carried out using the InterProScan web tool (http://www.ebi.ac.uk/interpro/).

DATA AND CODE AVAILABILITY

All sequencing data that support the findings of this study have been deposited in the National Genomics Data Center (NGDC) database with the accession number CRA006306.

SUPPLEMENTAL INFORMATION

Supplemental information is available at *Plant Communications Online*.

FUNDING

This work was supported by the National Natural Science Foundation of China (31872805), the Fundamental Research Funds for Central Non-Profit of the Chinese Academy of Agricultural Sciences (CAAS-ZDRW202109 and Y2023PT20), and the Nanfan Special Project of the Chinese Academy of Agricultural Sciences (YBXM15).

AUTHOR CONTRIBUTIONS

L.P. and J.S. conceived and designed the experiments. All authors performed the experiments and analyzed data. F.X., L.P., H.D., and J.S. wrote the paper. J.C.F. edited the paper. All authors read and approved the manuscript.

ACKNOWLEDGMENTS

We thank Prof. Lijia Qu (Peking University) for sharing the *Arabidopsis* transcription factor library used for yeast two-hybrid assays, Prof. Yunhai Li (Chinese Academy of Sciences) for providing seeds of *tcp14 tcp15* and *da1-ko1 dar1-1 dar2-1* mutants, Prof. Keke Yi (Institute of Agricultural Resources and Regional Planning of the Chinese Academy of Agricultural Sciences) and Prof. Lifang Niu (Biotechnology Research Institute of the Chinese Academy of Agricultural Sciences) for providing vectors, and Prof. Zinmay Renee Sung (University of California, Berkeley) for helpful comments on the manuscript. We also thank Rebeccagenome (Beijing, China) for high-throughput sequencing. No conflict of interest is declared.

Received: July 21, 2023
Revised: August 18, 2023
Accepted: January 9, 2024
Published: January 12, 2024

REFERENCES

Adhikari, P., Jain, R., Sharma, A., and Pandey, A. (2021). Plant Growth Promotion at Low Temperature by Phosphate-Solubilizing Pseudomonas Spp. Isolated from High-Altitude Himalayan Soil. Microb. Ecol. **82**:677–687.

Autran, D., Jonak, C., Belcram, K., Beemster, G.T., Kronenberger, J., Grandjean, O., Inze, D., and Traas, J. (2002). Cell numbers and leaf development in Arabidopsis: a functional analysis of the STRUWWELPETER gene. EMBO J. **21**:6036–6049.

Bainard, J.D., Newmaster, S.G., and Budke, J.M. (2020). Genome size and endopolyploidy evolution across the moss phylogeny. Ann. Bot. **125**:543–555.

Bertin, N. (2005). Analysis of the tomato fruit growth response to temperature and plant fruit load in relation to cell division, cell expansion and DNA endoreduplication. Ann. Bot. **95**:439–447.

Boudolf, V., Lammens, T., Boruc, J., Van Leene, J., Van Den Daele, H., Maes, S., Van Isterdael, G., Russinova, E., Kondorosi, E., Witters, E., et al. (2009). CDKB1;1 forms a functional complex with CYCA2;3 to suppress endocycle onset. Plant Physiol. **150**:1482–1493.

Breuer, C., Ishida, T., and Sugimoto, K. (2010). Developmental control of endocycles and cell growth in plants. Curr. Opin. Plant Biol. **13**:654–660.

Carles, C.C., and Fletcher, J.C. (2009). The SAND domain protein ULTRAPETALA1 acts as a trithorax group factor to regulate cell fate in plants. Genes Dev. **23**:2723–2728.

Carles, C.C., Lertpiriyapong, K., Reville, K., and Fletcher, J.C. (2004). The ULTRAPETALA1 gene functions early in Arabidopsis development to restrict shoot apical meristem activity and acts through WUSCHEL to regulate floral meristem determinacy. Genetics **167**:1893–1903.

Carles, C.C., Choffnes-Inada, D., Reville, K., Lertpiriyapong, K., and Fletcher, J.C. (2005). ULTRAPETALA1 encodes a SAND domain putative transcriptional regulator that controls shoot and floral meristem activity in Arabidopsis. Development **132**:897–911.

Chen, X., and Laux, T. (2012). Plant development–a snapshot in 2012. Curr. Opin. Plant Biol. **15**:1–3.

Chetverina, D.A., Mikhailova, A.V., Georgiev, P.G., and Erokhin, M.M. (2017). PRE/TRE elements act as transcription activators in Drosophila S2 Cells. Dokl. Biochem. Biophys. **472**:68–70.

Churchman, M.L., Brown, M.L., Kato, N., Kirik, V., Hülskamp, M., Inzé, D., De Veylder, L., Walker, J.D., Zheng, Z., Oppenheimer, D.G., et al. (2006). SIAMESE, a plant-specific cell cycle regulator, controls endoreplication onset in Arabidopsis thaliana. Plant Cell **18**:3145–3157.

Clay, N.K., and Nelson, T. (2005). The recessive epigenetic swellmap mutation affects the expression of two step II splicing factors required for the transcription of the cell proliferation gene STRUWWELPETER and for the timing of cell cycle arrest in the Arabidopsis leaf. Plant Cell **17**:1994–2008.

Clough, S.J., and Bent, A.F. (1998). Floral dip: a simplified method for Agrobacterium-mediated transformation of Arabidopsis thaliana. Plant J. **16**:735–743.

Cosgrove, D.J. (2000). Loosening of plant cell walls by expansins. Nature **407**:321–326.

de la Paz Sanchez, M., Aceves-García, P., Petrone, E., Steckenborn, S., Vega-León, R., Álvarez-Buylla, E.R., Garay-Arroyo, A., and García-Ponce, B. (2015). The impact of Polycomb group (PcG) and Trithorax group (TrxG) epigenetic factors in plant plasticity. New Phytol. **208**:684–694.

Dewitte, W., Riou-Khamlichi, C., Scofield, S., Healy, J.M.S., Jacqmard, A., Kilby, N.J., and Murray, J.A.H. (2003). Altered cell cycle distribution, hyperplasia, and inhibited differentiation in Arabidopsis caused by the D-type cyclin CYCD3. Plant Cell **15**:79–92.

Dinneny, J.R., Yadegari, R., Fischer, R.L., Yanofsky, M.F., and Weigel, D. (2004). The role of JAGGED in shaping lateral organs. Development **131**:1101–1110.

Disch, S., Anastasiou, E., Sharma, V.K., Laux, T., Fletcher, J.C., and Lenhard, M. (2006). The E3 ubiquitin ligase BIG BROTHER controls arabidopsis organ size in a dosage-dependent manner. Curr. Biol. **16**:272–279.

Dong, H., Liu, J., He, G., Liu, P., and Sun, J. (2020). Photoexcited phytochrome B interacts with brassinazole resistant 1 to repress brassinosteroid signaling in Arabidopsis. J. Integr. Plant Biol. **62**:652–667.

Dong, H., Dumenil, J., Lu, F.H., Na, L., Vanhaeren, H., Naumann, C., Klecker, M., Prior, R., Smith, C., McKenzie, N., et al. (2017). Ubiquitylation activates a peptidase that promotes cleavage and destabilization of its activating E3 ligases and diverse growth regulatory proteins to limit cell proliferation in Arabidopsis. Genes Dev. **31**:197–208.

Earley, K.W., Haag, J.R., Pontes, O., Opper, K., Juehne, T., Song, K., and Pikaard, C.S. (2006). Gateway-compatible vectors for plant functional genomics and proteomics. Plant J. **45**:616–629.

Fleming, A.J. (2006). The integration of cell proliferation and growth in leaf morphogenesis. J. Plant Res. **119**:31–36.

Fletcher, J.C. (2017). State of the Art: trxG Factor Regulation of Post-embryonic Plant Development. Front. Plant Sci. **8**:1925.

Förderer, A., Zhou, Y., and Turck, F. (2016). The age of multiplexity: recruitment and interactions of Polycomb complexes in plants. Curr. Opin. Plant Biol. **29**:169–178.

Gao, Q., Zhang, N., Wang, W.Q., Shen, S.Y., Bai, C., and Song, X.J. (2021). The ubiquitin-interacting motif-type ubiquitin receptor HDR3 interacts with and stabilizes the histone acetyltransferase GW6a to control the grain size in rice. Plant Cell **33**:3331–3347.

Gastaldi, V., Lucero, L.E., Ferrero, L.V., Ariel, F.D., and Gonzalez, D.H. (2020). Class-I TCP Transcription Factors Activate the SAUR63 Gene Subfamily in Gibberellin-Dependent Stamen Filament Elongation. Plant Physiol. **182**:2096–2110.

Gonzalez, N., Vanhaeren, H., and Inzé, D. (2012). Leaf size control: complex coordination of cell division and expansion. Trends Plant Sci. **17**:332–340.

Guo, A.Y., Zhu, Q.H., Chen, X., and Luo, J.C. (2007). [GSDS: a gene structure display server]. Yi Chuan **29**:1023–1026.

Hao, J., Wang, D., Wu, Y., Huang, K., Duan, P., Li, N., Xu, R., Zeng, D., Dong, G., Zhang, B., et al. (2021). The GW2-WG1-OsbZIP47 pathway controls grain size and weight in rice. Mol. Plant **14**:1266–1280.

Hecker, A., Brand, L.H., Peter, S., Simoncello, N., Kilian, J., Harter, K., Gaudin, V., and Wanke, D. (2015). The Arabidopsis GAGA-Binding Factor BASIC PENTACYSTEINE6 Recruits the POLYCOMB-REPRESSIVE COMPLEX1 Component LIKE HETEROCHROMATIN PROTEIN1 to GAGA DNA Motifs. Plant Physiol. **168**:1013–1024.

Heo, J.B., and Sung, S. (2011). Vernalization-mediated epigenetic silencing by a long intronic noncoding RNA. Science **331**:76–79.

Horiguchi, G., Kim, G.T., and Tsukaya, H. (2005). The transcription factor AtGRF5 and the transcription coactivator AN3 regulate cell proliferation in leaf primordia of Arabidopsis thaliana. Plant J. **43**:68–78.

Imai, K.K., Ohashi, Y., Tsuge, T., Yoshizumi, T., Matsui, M., Oka, A., and Aoyama, T. (2006). The A-type cyclin CYCA2;3 is a key regulator of ploidy levels in Arabidopsis endoreduplication. Plant Cell **18**:382–396.

Jiang, B., Lv, Q., Wan, W., Le, L., Xu, L., Hu, K., and Xiao, P. (2018). Transcriptome analysis reveals the mechanism of the effect of flower tea Coreopsis tinctoria on hepatic insulin resistance. Food Funct. **9**:5607–5620.

Kassis, J.A., and Brown, J.L. (2013). Polycomb group response elements in Drosophila and vertebrates. Adv. Genet. **81**:83–118.

Kawade, K., Horiguchi, G., Usami, T., Hirai, M.Y., and Tsukaya, H. (2013). ANGUSTIFOLIA3 signaling coordinates proliferation between clonally distinct cells in leaves. Curr. Biol. **23**:788–792.

Kieffer, M., Master, V., Waites, R., and Davies, B. (2011). TCP14 and TCP15 affect internode length and leaf shape in Arabidopsis. Plant J. **68**:147–158.

Kim, D.H., and Sung, S. (2017). Vernalization-Triggered Intragenic Chromatin Loop Formation by Long Noncoding RNAs. Dev. Cell **40**:302–312.e4.

Kim, J.H., Choi, D., and Kende, H. (2003). The AtGRF family of putative transcription factors is involved in leaf and cotyledon growth in Arabidopsis. Plant J. **36**:94–104.

Kingston, R.E., and Tamkun, J.W. (2014). Transcriptional regulation by trithorax-group proteins. Cold Spring Harbor Perspect. Biol. **6**:a019349.

Kocova, V., Strakova, N., Kolarcik, V., Rakai, A., and Martonfi, P. (2016). Endoreduplication as a part of flower ontogeny in Trifolium pratense cultivars. Bot. Stud. **57**:1–8.

Krizek, B.A. (1999). Ectopic expression of AINTEGUMENTA in Arabidopsis plants results in increased growth of floral organs. Dev. Genet. **25**:224–236.

Kumar, S., Stecher, G., Li, M., Knyaz, C., and Tamura, K. (2018). MEGA X: Molecular Evolutionary Genetics Analysis across Computing Platforms. Mol. Biol. Evol. **35**:1547–1549.

Lammens, T., Boudolf, V., Kheibarshekan, L., Zalmas, L.P., Gaamouche, T., Maes, S., Vanstraelen, M., Kondorosi, E., La Thangue, N.B., Govaerts, W., et al. (2008). Atypical E2F activity restrains APC/CCCS52A2 function obligatory for endocycle onset. Proc. Natl. Acad. Sci. USAUSA **105**:14721–14726.

Li, C., Chen, C., Gao, L., Yang, S., Nguyen, V., Shi, X., Siminovitch, K., Kohalmi, S.E., Huang, S., Wu, K., et al. (2015). The Arabidopsis SWI2/SNF2 chromatin Remodeler BRAHMA regulates polycomb function during vegetative development and directly activates the flowering repressor gene SVP. PLoS Genet. **11**, e1004944.

Li, Y., Zheng, L., Corke, F., Smith, C., and Bevan, M.W. (2008). Control of final seed and organ size by the DA1 gene family in Arabidopsis thaliana. Genes Dev. **22**:1331–1336.

Li, Z., Li, B., Liu, J., Guo, Z., Liu, Y., Li, Y., Shen, W.H., Huang, Y., Huang, H., Zhang, Y., and Dong, A. (2016). Transcription factors AS1 and AS2 interact with LHP1 to repress KNOX genes in Arabidopsis. J. Integr. Plant Biol. **58**:959–970.

Li, Z.Y., Li, B., and Dong, A.W. (2012). The Arabidopsis transcription factor AtTCP15 regulates endoreduplication by modulating expression of key cell-cycle genes. Mol. Plant **5**:270–280.

Liu, J., Zhang, T., Jia, J., and Sun, J. (2016). The Wheat Mediator Subunit TaMED25 Interacts with the Transcription Factor TaEIL1 to Negatively Regulate Disease Resistance against Powdery Mildew. Plant Physiol. **170**:1799–1816.

Liu, Z., Chen, G., Gao, F., Xu, R., Li, N., Zhang, Y., and Li, Y. (2019). Transcriptional Repression of the APC/C Activator Genes CCS52A1/A2 by the Mediator Complex Subunit MED16 Controls Endoreduplication and Cell Growth in Arabidopsis. Plant Cell **31**:1899–1912.

Lyu, J., Wang, D., Duan, P., Liu, Y., Huang, K., Zeng, D., Zhang, L., Dong, G., Li, Y., Xu, R., et al. (2020). Control of Grain Size and Weight by the GSK2-LARGE1/OML4 Pathway in Rice. Plant Cell **32**:1905–1918.

Ma, N., Wang, Y., Qiu, S., Kang, Z., Che, S., Wang, G., and Huang, J. (2013). Overexpression of OsEXPA8, a root-specific gene, improves rice growth and root system architecture by facilitating cell extension. PLoS One **8**, e75997.

Magyar, Z., Horváth, B., Khan, S., Mohammed, B., Henriques, R., De Veylder, L., Bakó, L., Scheres, B., and Bögre, L. (2012). Arabidopsis E2FA stimulates proliferation and endocycle separately through RBR-bound and RBR-free complexes. EMBO J. **31**:1480–1493.

Martín-Trillo, M., and Cubas, P. (2010). TCP genes: a family snapshot ten years later. Trends Plant Sci. **15**:31–39.

Mizukami, Y. (2001). A matter of size: developmental control of organ size in plants. Curr. Opin. Plant Biol. **4**:533–539.

Mizukami, Y., and Fischer, R.L. (2000). Plant organ size control: AINTEGUMENTA regulates growth and cell numbers during organogenesis. Proc. Natl. Acad. Sci. USAUSA **97**:942–947.

Monfared, M.M., Carles, C.C., Rossignol, P., Pires, H.R., and Fletcher, J.C. (2013). The ULT1 and ULT2 trxG genes play overlapping roles in Arabidopsis development and gene regulation. Mol. Plant **6**:1564–1579.

Moreau, F., Thévenon, E., Blanvillain, R., Lopez-Vidriero, I., Franco-Zorrilla, J.M., Dumas, R., Parcy, F., Morel, P., Trehin, C., and Carles, C.C. (2016). The Myb-domain protein ULTRAPETALA1 INTERACTING FACTOR 1 controls floral meristem activities in Arabidopsis. Development **143**:1108–1119.

Ornelas-Ayala, D., Vega-León, R., Petrone-Mendoza, E., Garay-Arroyo, A., García-Ponce, B., Álvarez-Buylla, E.R., and Sanchez, M.d.l.P. (2020). ULTRAPETALA1 maintains Arabidopsis root stem cell niche independently of ARABIDOPSIS TRITHORAX1. New Phytol. **225**:1261–1272.

Ou, B., Yin, K.Q., Liu, S.N., Yang, Y., Gu, T., Wing Hui, J.M., Zhang, L., Miao, J., Kondou, Y., Matsui, M., et al. (2011). A high-throughput screening system for Arabidopsis transcription factors and its application to Med25-dependent transcriptional regulation. Mol. Plant **4**:546–555.

Peng, Y., Chen, L., Lu, Y., Wu, Y., Dumenil, J., Zhu, Z., Bevan, M.W., and Li, Y. (2015). The ubiquitin receptors DA1, DAR1, and DAR2 redundantly regulate endoreduplication by modulating the stability of TCP14/15 in Arabidopsis. Plant Cell **27**:649–662.

Pérez-Pérez, J.M., Candela, H., and Micol, J.L. (2009). Understanding synergy in genetic interactions. Trends Genet. **25**:368–376.

Pires, H.R., Monfared, M.M., Shemyakina, E.A., and Fletcher, J.C. (2014). ULTRAPETALA trxG genes interact with KANADI transcription factor genes to regulate Arabidopsis gynoecium patterning. Plant Cell **26**:4345–4361.

Pu, L., and Sung, Z.R. (2015). PcG and trxG in plants - friends or foes. Trends Genet. **31**:252–262.

Pu, L., Liu, M.S., Kim, S.Y., Chen, L.F.O., Fletcher, J.C., and Sung, Z.R. (2013). EMBRYONIC FLOWER1 and ULTRAPETALA1 Act Antagonistically on Arabidopsis Development and Stress Response. Plant Physiol. **162**:812–830.

Roy, D., Chakrabarty, J., Mallik, R., and Chaudhuri, S. (2019). Rice Trithorax factor ULTRAPETALA 1 (OsULT1) specifically binds to "GAGAG" sequence motif present in Polycomb response elements. Biochim. Biophys. Acta. Gene Regul. Mech. **1862**:582–597.

Saleh, A., Al-Abdallat, A., Ndamukong, I., Alvarez-Venegas, R., and Avramova, Z. (2007). The Arabidopsis homologs of trithorax (ATX1) and enhancer of zeste (CLF) establish 'bivalent chromatin marks' at the silent AGAMOUS locus. Nucleic Acids Res. **35**:6290–6296.

Sasidharan, R., and Pierik, R. (2010). Cell wall modification involving XTHs controls phytochrome-mediated petiole elongation in Arabidopsis thaliana. Plant Signal. Behav. **5**:1491–1492.

Schnablová, R., Herben, T., and Klimešová, J. (2017). Shoot apical meristem and plant body organization: a cross-species comparative study. Ann. Bot. **120**:833–843.

Schuettengruber, B., Bourbon, H.M., Di Croce, L., and Cavalli, G. (2017). Genome Regulation by Polycomb and Trithorax: 70 Years and Counting. Cell **171**:34–57.

Shpak, E.D., Berthiaume, C.T., Hill, E.J., and Torii, K.U. (2004). Synergistic interaction of three ERECTA-family receptor-like kinases controls Arabidopsis organ growth and flower development by promoting cell proliferation. Development **131**:1491–1501.

Sugimoto-Shirasu, K., and Roberts, K. (2003). "Big it up": endoreduplication and cell-size control in plants. Curr. Opin. Plant Biol. **6**:544–553.

Szécsi, J., Joly, C., Bordji, K., Varaud, E., Cock, J.M., Dumas, C., and Bendahmane, M. (2006). BIGPETALp, a bHLH transcription factor is involved in the control of Arabidopsis petal size. EMBO J. **25**:3912–3920.

Tian, Y., Zheng, H., Zhang, F., Wang, S., Ji, X., Xu, C., He, Y., and Ding, Y. (2019). PRC2 recruitment and H3K27me3 deposition at FLC require FCA binding of COOLAIR. Sci. Adv. **5**:eaau7246.

Vanhaeren, H., Nam, Y.J., De Milde, L., Chae, E., Storme, V., Weigel, D., Gonzalez, N., and Inzé, D. (2017). Forever Young: The Role of Ubiquitin Receptor DA1 and E3 Ligase BIG BROTHER in Controlling Leaf Growth and Development. Plant Physiol. **173**:1269–1282.

Vanhaeren, H., Chen, Y., Vermeersch, M., De Milde, L., De Vleeschhauwer, V., Natran, A., Persiau, G., Eeckhout, D., De Jaeger, G., Gevaert, K., et al. (2020). UBP12 and UBP13 negatively regulate the activity of the ubiquitin-dependent peptidases DA1, DAR1 and DAR2. Elife **9**, 52276.

Wang, H., Fowke, L.C., and Crosby, W.L. (1997). A plant cyclin-dependent kinase inhibitor gene. Nature **386**:451–452.

Wang, X., Fan, C., Zhang, X., Zhu, J., and Fu, Y.F. (2013). BioVector, a flexible system for gene specific-expression in plants. BMC Plant Biol. **13**:198.

Wang, Z., Li, N., Jiang, S., Gonzalez, N., Huang, X., Wang, Y., Inzé, D., and Li, Y. (2016). SCF(SAP) controls organ size by targeting PPD proteins for degradation in Arabidopsis thaliana. Nat. Commun. **7**, 11192.

White, D.W.R. (2006). PEAPOD regulates lamina size and curvature in Arabidopsis. Proc. Natl. Acad. Sci. USAUSA **103**:13238–13243.

Wieters, B., Steige, K.A., He, F., Koch, E.M., Ramos-Onsins, S.E., Gu, H., Guo, Y.L., Sunyaev, S., and de Meaux, J. (2021). Polygenic adaptation of rosette growth in Arabidopsis thaliana. PLoS Genet. **17**, e1008748.

Willems, A., Heyman, J., Eekhout, T., Achon, I., Pedroza-Garcia, J.A., Zhu, T., Li, L., Vercauteren, I., Van den Daele, H., van de Cotte, B., et al. (2020). The Cyclin CYCA3;4 Is a Postprophase Target of the APC/C(CCS52A2) E3-Ligase Controlling Formative Cell Divisions in Arabidopsis. Plant Cell **32**:2979–2996.

Wu, M.F., Sang, Y., Bezhani, S., Yamaguchi, N., Han, S.K., Li, Z., Su, Y., Slewinski, T.L., and Wagner, D. (2012). SWI2/SNF2 chromatin remodeling ATPases overcome polycomb repression and control floral organ identity with the LEAFY and SEPALLATA3 transcription factors. Proc. Natl. Acad. Sci. USAUSA **109**:3576–3581.

Wu, S.Z., and Bezanilla, M. (2018). Actin and microtubule cross talk mediates persistent polarized growth. J. Cell Biol. **217**:3531–3544.

Wuarin, J., Buck, V., Nurse, P., and Millar, J.B.A. (2002). Stable association of mitotic cyclin B/Cdc2 to replication origins prevents endoreduplication. Cell **111**:419–431.

Xia, T., Li, N., Dumenil, J., Li, J., Kamenski, A., Bevan, M.W., Gao, F., and Li, Y. (2013). The ubiquitin receptor DA1 interacts with the E3 ubiquitin ligase DA2 to regulate seed and organ size in Arabidopsis. Plant Cell **25**:3347–3359.

Xie, G., Li, Z., Ran, Q., Wang, H., and Zhang, J. (2018). Over-expression of mutated ZmDA1 or ZmDAR1 gene improves maize kernel yield by enhancing starch synthesis. Plant Biotechnol. J. **16**:234–244.

Xu, F., Kuo, T., Rosli, Y., Liu, M.S., Wu, L., Chen, L.F.O., Fletcher, J.C., Sung, Z.R., and Pu, L. (2018a). Trithorax Group Proteins Act Together with a Polycomb Group Protein to Maintain Chromatin Integrity for Epigenetic Silencing during Seed Germination in Arabidopsis. Mol. Plant **11**:659–677.

Xu, R., Duan, P., Yu, H., Zhou, Z., Zhang, B., Wang, R., Li, J., Zhang, G., Zhuang, S., Lyu, J., et al. (2018b). Control of Grain Size and Weight by the OsMKKK10-OsMKK4-OsMAPK6 Signaling Pathway in Rice. Mol. Plant **11**:860–873.

Yuan, L., Song, X., Zhang, L., Yu, Y., Liang, Z., Lei, Y., Ruan, J., Tan, B., Liu, J., and Li, C. (2021). The transcriptional repressors VAL1 and VAL2 recruit PRC2 for genome-wide Polycomb silencing in Arabidopsis. Nucleic Acids Res. **49**:98–113.

Zhang, X., Bernatavichute, Y.V., Cokus, S., Pellegrini, M., and Jacobsen, S.E. (2009). Genome-wide analysis of mono-di- and trimethylation of histone H3 lysine 4 in Arabidopsis thaliana. Genome Biol. **10**:R62.

Zhang, X., Guo, W., Du, D., Pu, L., and Zhang, C. (2020). Overexpression of a maize BR transcription factor ZmBZR1 in Arabidopsis enlarges organ and seed size of the transgenic plants. Plant Sci. **292**, 110378.